

# Quantum algorithms to simulate many-body physics of correlated fermions

Zhang Jiang,<sup>1,2,\*</sup> Kevin J. Sung,<sup>3</sup> Kostyantyn Kechedzhi,<sup>1,4</sup> Vadim N. Smelyanskiy,<sup>5</sup> and Sergio Boixo<sup>5</sup>

<sup>1</sup>NASA Ames Research Center Quantum Artificial Intelligence Laboratory (QuAIL), Moffett Field, CA 94035, USA

<sup>2</sup>Stinger Ghaffarian Technologies Inc., 7701 Greenbelt Road, Suite 400, Greenbelt, MD 20770, USA

<sup>3</sup>Department of Electrical Engineering and Computer Science University of Michigan, Ann Arbor, MI 48109, USA

<sup>4</sup>USRA, NASA Ames Research Center, Moffett Field, CA 94035

<sup>5</sup>Google, Venice, CA 90291, USA

(Dated: May 6, 2022)

Simulating strongly correlated fermionic systems is notoriously hard on classical computers. An alternative approach, as proposed by Feynman, is to use a quantum computer. Here, we discuss quantum simulation of strongly correlated fermionic systems. We focus specifically on 2D and linear geometry with nearest neighbor qubit-qubit couplings, typical for superconducting transmon qubit arrays. We improve an existing algorithm to prepare an arbitrary Slater determinant by exploiting a unitary symmetry. We also present a quantum algorithm to prepare an arbitrary fermionic Gaussian state with  $O(N^2)$  gates and  $O(N)$  circuit depth. Both algorithms are optimal in the sense that the numbers of parameters in the quantum circuits are equal to those to describe the quantum states. Furthermore, we propose an algorithm to implement the 2-dimensional (2D) fermionic Fourier transformation on a 2D qubit array with only  $O(N^{1.5})$  gates and  $O(\sqrt{N})$  circuit depth, which is the minimum depth required for quantum information to travel across the qubit array. We also present methods to simulate each time step in the evolution of the 2D Fermi-Hubbard model—again on a 2D qubit array—with  $O(N)$  gates and  $O(\sqrt{N})$  circuit depth. Finally, we discuss how these algorithms can be used to determine the ground state properties and phase diagrams of strongly correlated quantum systems using the Hubbard model as an example.

## I. INTRODUCTION

A large class of materials evade description by density functional theory (DFT) [1] due to the effects of strong electron-electron correlations [2, 3]. Simulation of strongly correlated electronic structure and dynamical effects in such materials would allow quantitative prediction of their physical characteristics before fabricating them, which is often costly. This would open the route for designing materials with application-specific characteristics. The properties of strongly correlated fermionic systems remain elusive after many years of intense research. Indeed, solving a general quantum many-body problem without using approximations on a classical computer takes exponential time in the size of problem. One way to avoid this difficulty, as envisioned by Feynman, is to use a quantum computer to simulate quantum systems [4, 5]. In experiments with real materials, one rarely knows for sure the initial states and the underlying Hamiltonians. A quantum computer, however, enables one to prepare the initial state with confidence and to have full control over the Hamiltonian under which the state evolves. We are closer to Feynman’s vision with recent advances in quantum computing hardware. It is important to develop simulation algorithms optimized given the limitations of current and near-term quantum hardware, such as locality of qubit-qubit couplings, gate sequences, and mitigation of errors and noise. Significant progress has been made in this direction [6–9]. In this paper we propose several quantum algorithms to simulate correlated fermions

on 2D and linear qubit arrays with nearest-neighbor couplings which are typical for superconducting transmon qubits. We use the Fermi-Hubbard model as an example to demonstrate these algorithms. In this simple model, the superconducting to Mott insulator transition is solely determined by the competition between the hopping and the interaction terms. Solving the Hubbard model allows one to single out this mechanism from other effects such as disorder and long-range interactions in real materials.

The Hubbard model [10] approximates the long-range Coulomb interaction of electrons in a crystal with local on-site interaction. This locality reduces the resources required for simulating the model and makes it a prime candidate for the early applications of quantum simulations [11]. The single-band Fermi-Hubbard model is described by the Hamiltonian,

$$\mathcal{H}_{\text{FH}} = - \sum_{\langle j,k \rangle, \sigma} t_{jk} (c_{j,\sigma}^\dagger c_{k,\sigma} + \text{h.c.}) + U \sum_j n_{j,\uparrow} n_{j,\downarrow} + \sum_{j,\sigma} (\epsilon_j - \mu) n_{j,\sigma} - \sum_j h_j (n_{j,\uparrow} - n_{j,\downarrow}), \quad (1)$$

where  $c_{j,\sigma}^\dagger$  ( $c_{j,\sigma}$ ) is the creation (annihilation) operator for the  $j$ th site with spin  $\sigma$  and  $n_{j,\sigma} = c_{j,\sigma}^\dagger c_{j,\sigma}$  is the fermion occupation number operator. The first term on the right side of Eq. (1) describes fermions hopping between sites, the second term describes the on-site interactions, and the remaining two terms describe a local potential and a magnetic field. The model demonstrates a wide range of strongly correlated phenomena, including metal-insulator transitions, unconventional Fermi liquids, and a number of inhomogeneous phases. The Fermi-Hubbard model also provides an approximate description

\* zhang.jiang@nasa.gov

of materials [12] including the cuprate family [13] (albeit a multi-band extension of the model is necessary for quantitative correspondence to the materials), which has attracted a lot of interest because of unconventional symmetry breaking phenomena and high-temperature superconductivity [14].

The 1-dimensional (1D) Hubbard model was solved by Lieb and Wu in 1968 [15]; however, full theoretical analysis of 2D Hubbard model requires going beyond the validity of meanfield and perturbation theory arguments and remains an open question. The 2D Hubbard model serves as a canonical microscopic physical model for strongly correlated fermionic systems. In the underdoped region of its phase diagram, multiple orders exist corresponding to a regime of maximum numerical difficulty. Significant numerical progress has been made in the identification of the unconventional Mott-insulator transition and a superconducting phase with  $d$ -wave order parameter [16, 17]. Exact numerical diagonalization is limited to  $\sim 20$  sites (40 logical qubits) [18, 19], which is too small for finite size scaling analysis. Approximate methods such as quantum Monte Carlo simulations or many-body theory expansions have been used to simulate systems with hundreds of sites, which allows for extrapolation to the thermodynamic limit. Except at half filling, quantum Monte Carlo methods suffer from sign problems which prevent them from simulating systems at very low temperatures [20]. Application of the density matrix renormalization group (DMRG) [21] to the 2D Hubbard model requires mapping to an effective 1D problem, to which the standard DMRG is applied. Other numerical methods to determine the phase diagrams of the Hubbard model include the dynamical cluster approximation (DCA) [22, 23] and the density matrix embedding theory (DMET) [17, 24]. These methods can asymptotically approach the exact solution with increasingly larger clusters, however, simulating those clusters requires an exponential amount of computing resources on a classical computer.

To simulate the Fermi-Hubbard model on a quantum computer, one needs to map the fermionic operators to qubit operators. In the second quantization picture, a particular spin orbital being unoccupied or occupied can be represented by the qubit states  $|0\rangle$  or  $|1\rangle$ , respectively. To retain the fermionic anticommutation relations, one also needs to account for the parities of qubits corresponding to other spin orbitals, e.g., by using the Jordan-Wigner transformation (JWT) [25, 26]. The two terms in the second line of Eq. (1) can be implemented using only single-qubit operators, and the on-site interaction term can be implemented with two-qubit interactions. The hopping terms, however, cannot be implemented straightforwardly in more than one spatial dimension because of the nonlocal parity operators in the JWT. It is of practical importance to reduce the depth of the quantum circuits for these terms with only local qubit interactions [9], which is crucial to near-term quantum computers without quantum error correction [27, 28]. We

will always have local qubit interactions in mind, which is a different model from quantum computation with all-to-all interactions. The digital quantum simulations we consider here could address low-temperature properties of the Hubbard model which so far remain hard to access with analog simulators [29]. In addition to simulating unitary dynamics, preparing the ground state is a source of significant overhead in digital quantum simulations. We develop algorithms for state preparations with only locally coupled qubits by adopting the general ideas in Ref. [11].

Beyond the Hubbard model there are a growing number of materials showing surprising sensitivity to impurities, it is an open issue to understand and ultimately to control the emergent phases from impurities [30]. At low temperatures, impurities and disorder can induce a metal-to-insulator transition by localizing the Cooper pairs [31, 32]. Impurities, however, can also induce interesting new phases of strongly correlated matter and help probe the underlying mechanism of exotic states [33, 34]. On the other hand, quantum impurity models are useful for hybrid quantum-classical approaches to strongly correlated materials [35], where the quantum computer solves an impurity problem that is determined self-consistently with the help of a classical computer. Our methods work for systems that violate translational symmetries and thus are suited for simulating impurity models.

In Section II, we review the topic of mapping fermionic operators to qubit operators and introduce notations. In Section III, we improve an existing quantum algorithm in Ref. [11] to prepare an arbitrary Slater determinant by exploiting a unitary symmetry. In Section IV, we present an algorithm to prepare an arbitrary fermionic Gaussian state, improving and generalizing an existing method for translationally invariant systems [36]. Both algorithms in Sections III and IV have been implemented as part of the open-source project OpenFermion [37]. In Section V, we introduce a quantum algorithm to implement the 2D fermionic Fourier transformation on a 2D qubit array with only  $O(N^{1.5})$  gates and  $O(\sqrt{N})$  circuit depth, a better scaling than methods based on the fermionic SWAP gates [9]. In Section VI, we discuss applications of our quantum algorithms using the Fermi-Hubbard model as an example. In Appendix A, we review the properties of meanfield Hamiltonians that are quadratic in the fermionic creation and annihilation operators and how to diagonalize these Hamiltonians. In Appendix B, we introduce an alternative approach to solve time evolutions of the quantum lattice models, such as the Hubbard model, by using ancilla-assisted fermionic gates. In Appendix C, we discuss fermionic operations based on Hamiltonian evolution. In Appendix D, we briefly review the fermionic SWAP gate. In Appendix E, we discuss how to simulate the 2D Hubbard model with a qubit ladder using the fermionic SWAP gate. In Appendix F, we study the Trotter errors in adiabatic state preparation numerically for small system sizes.

## II. MAPPING FERMIONS TO QUBITS

The first step in solving strongly correlated fermionic systems with a quantum computer is to map the Hilbert space of fermions to the states of qubits. Following Ref. [38], we represent the fermionic Hamiltonian in the second quantization picture using a discrete basis of spin orbitals. A qubit is assigned to each spin orbital; the qubit state  $|0\rangle$  or  $|1\rangle$  denotes an unoccupied or occupied spin orbital, respectively. The fermionic operators satisfying the anticommutation relations can be mapped to qubit operators using either the Jordan-Wigner transformation (JWT) [25, 26], the Bravyi-Kitaev transformation (BKT) [39, 40], or the Verstraete-Cirac transformation (VCT) [41]. To represent the parities, the JWT requires strings of Pauli operators that act on  $O(N)$  qubits, the BKT uses  $O(\log N)$  nonlocal operators, and the VCT requires only  $O(1)$  local operators by introducing one ancilla qubit per logical qubit. Although the JWT seems to have the worst scaling, it has the most straightforward form and can be applied to 1D fermionic systems without encountering the parity problem. One way to get around the parity problem in the JWT for systems of higher dimensions is to use fermionic SWAP gates [9, 42]. We will discuss a different approach based on traveling ancilla qubits, which solves the parity problem in the JWT with negligible overhead.

The JWT maps the fermionic creation and annihilation operators to qubit operators as follows:

$$c_j^\dagger \mapsto \frac{1}{2} (X_j - iY_j) Z_1 \cdots Z_{j-1}, \quad (2a)$$

$$c_j \mapsto \frac{1}{2} (X_j + iY_j) Z_1 \cdots Z_{j-1}, \quad (2b)$$

where  $X$ ,  $Y$ , and  $Z$  are the Pauli operators. It assumes an ordering of the qubits and attaches the Pauli- $Z$  operators with smaller indices (the parity) to the raising and lowering operators. A single Slater determinant in the computational basis (Fock state) takes the form

$$c_{j_1}^\dagger \cdots c_{j_{N_f}}^\dagger |\text{vac}\rangle \mapsto \left( \prod_{n=1}^{N_f} \frac{X_{j_n} - iY_{j_n}}{2} \right) |0 \cdots 0\rangle, \quad (3)$$

where  $j_1 < j_2 < \cdots < j_{N_f}$  and  $|\text{vac}\rangle$  is the vacuum state. The fermionic number operator

$$c_j^\dagger c_j \mapsto \frac{1}{4} (X_j - iY_j)(X_j + iY_j) = \frac{1}{2} (I - Z_j), \quad (4)$$

where  $I$  is the  $2 \times 2$  identity operator. The fermionic hopping term can be realized by a product of Pauli operators ( $k > j$ ),

$$c_j^\dagger c_k \mapsto \frac{1}{4} (X_j - iY_j)(X_k + iY_k) Z_{j+1} \cdots Z_{k-1}. \quad (5)$$

For the case  $k = j + 1$ , we have

$$-i(c_j^\dagger c_{j+1} - \text{h.c.}) \mapsto \frac{1}{2} (X_j Y_{j+1} - Y_j X_{j+1}), \quad (6a)$$

$$c_j^\dagger c_{j+1} + \text{h.c.} \mapsto \frac{1}{2} (X_j X_{j+1} + Y_j Y_{j+1}), \quad (6b)$$

interactions which can be implemented efficiently with superconducting qubits [43]. The hopping terms between orbitals encoded far apart from each other in the Jordan-Wigner transformation, however, are generally hard to implement. In Sections III and IV, we discuss state preparation algorithms that totally avoid such hopping terms. In Section V and Appendix B, we also discuss strategies to implement such terms by introducing ancilla qubits that store the parities.

## III. PREPARING SLATER DETERMINANTS

A Slater determinant can be regarded as an eigenstate of a Hamiltonian quadratic in fermionic creation and annihilation operators, or simply quadratic Hamiltonian. The standard algorithm to prepare Slater determinants was described in Ref. [25] and improved in Ref. [11] using elementary operations called Givens rotations, which are rotations in the plane spanned by two coordinates axes. The circuit depth and implementability can be improved by parallelizing the Givens rotations restricted to neighboring qubits [42]. Here, we present an algorithm that reduces the total number of Givens rotations by exploiting a freedom in the representation of Slater determinants; Python code for this algorithm is available as part of the OpenFermion project [37].

In the second quantization picture, a single Slater determinant takes the form

$$|\Psi_S\rangle = b_1^\dagger \cdots b_{N_f}^\dagger |\text{vac}\rangle, \quad b_j^\dagger = \sum_{k=1}^N Q_{jk} c_k^\dagger, \quad (7)$$

where  $Q$  is an  $N_f \times N$  matrix satisfying

$$Q^\dagger Q = P_S, \quad (8)$$

with  $P_S$  the projector (of rank  $N_f$ ) onto the subspace spanned by the single-particle wavefunctions of the occupied spin orbitals (rows of  $Q$ ). An arbitrary Slater determinant (7) can be prepared by applying a single-particle basis change  $\mathcal{U}$  to an easy-to-prepare determinant in the computational basis (3):

$$|\Psi_S\rangle = \mathcal{U} c_1^\dagger \cdots c_{N_f}^\dagger |\text{vac}\rangle, \quad \mathcal{U} c_j^\dagger \mathcal{U}^\dagger = b_j^\dagger, \quad (9)$$

for  $j = 1, 2, \dots, N_f$ . The unitary  $\mathcal{U}$  corresponds to a fermionic Fourier transformation when the rows of  $Q$  are orthonormal plane waves. The identity (8) remains true under the transformation  $Q \rightarrow VQ$ , where  $V$  is an arbitrary  $N_f \times N_f$  unitary matrix. Indeed, the Slater determinant (7) remains the same (up to an overall phase)

under the basis transformation  $V$ :

$$\left( \prod_{j=1}^{N_f} \sum_{k=1}^{N_f} V_{jk} b_k^\dagger \right) |\text{vac}\rangle = \det(V) |\Psi_S\rangle, \quad (10)$$

where  $\det(V)$  is the determinant of  $V$ . The unitary  $V$  can be chosen to be composed of a sequence of Givens rotations on neighboring rows of  $Q$  that bring the matrix elements in its upper right corner to zeros. A Givens rotation takes the following form in the two relevant coordinate axes:

$$\begin{aligned} G(\theta, \varphi) &= \begin{pmatrix} \cos \theta & -e^{i\varphi} \sin \theta \\ \sin \theta & e^{i\varphi} \cos \theta \end{pmatrix} \\ &= \begin{pmatrix} \cos \theta & -\sin \theta \\ \sin \theta & \cos \theta \end{pmatrix} \begin{pmatrix} 1 & 0 \\ 0 & e^{i\varphi} \end{pmatrix}, \end{aligned} \quad (11)$$

where we have generalized the original definition by allowing complex matrix elements. For example, with  $N = 6$  and  $N_f = 3$ , we can break  $V$  into three Givens rotations,

$$\begin{aligned} Q &\rightarrow \begin{pmatrix} * & * & * & * & * & 0 \\ * & * & * & * & * & * \\ * & * & * & * & * & * \\ * & * & * & * & * & * \end{pmatrix} \rightarrow \begin{pmatrix} * & * & * & * & * & 0 \\ * & * & * & * & * & 0 \\ * & * & * & * & * & * \\ * & * & * & * & * & * \end{pmatrix} \\ &\rightarrow \begin{pmatrix} * & * & * & * & 0 & 0 \\ * & * & * & * & * & * \\ * & * & * & * & * & * \\ * & * & * & * & * & * \end{pmatrix} = VQ, \end{aligned} \quad (12)$$

where  $*$  represents an arbitrary matrix element, and the red-colored matrix elements are zeroed out with Givens rotations. This procedure does not change the Slater determinant (10) and no physical operation is required. However, it makes it clear that the number of physical Givens rotations can be reduced and how this can be achieved.

The unitary in Eq. (9) corresponds to a single-particle basis change and can be decomposed into a sequence of Givens rotations [11],

$$U = \mathcal{G}_1 \mathcal{G}_2 \cdots \mathcal{G}_{N_G}. \quad (13)$$

The Givens rotation  $\mathcal{G}(\theta, \varphi)$  acting on the  $j$ th and  $k$ th spin orbitals takes the form

$$\begin{pmatrix} \mathcal{G} c_j^\dagger \mathcal{G}^\dagger \\ \mathcal{G} c_k^\dagger \mathcal{G}^\dagger \end{pmatrix} = G(\theta, \varphi) \begin{pmatrix} c_j^\dagger \\ c_k^\dagger \end{pmatrix}, \quad (14)$$

where the  $2 \times 2$  matrix  $G(\theta, \varphi)$  is defined in Eq. (11). A Givens rotation of the form (14) can be implemented on a quantum computer using the circuit in Fig. 1 (the two qubits are adjacent in the JWT). The first part of the circuit (dotted box) describes to a rotation between the qubit states  $|10\rangle$  and  $|01\rangle$  corresponding a rotation in the single-particle subspace of the two spin orbitals; the two qubit states  $|00\rangle$  and  $|11\rangle$  corresponding to the unoccupied state and the double-occupied state are unchanged in this step. The fermionic unitary  $\mathcal{U}$  in Eq. (13)

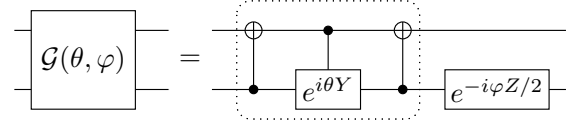


FIG. 1. Quantum circuit for a Givens rotation on neighboring qubits: the part in dotted box represents a rotation between the two states  $|01\rangle$  and  $|10\rangle$ .

can be represented by a matrix  $U$  corresponding to a single-particle basis change, see Appendix A,

$$\mathcal{U} \mathbf{c}^\dagger \mathcal{U}^\dagger = U \mathbf{c}^\dagger, \quad U = G_{N_G} \cdots G_2 G_1, \quad (15)$$

where  $\mathbf{c}^\dagger = (c_1^\dagger \cdots c_N^\dagger)^T$ . The order of the Givens rotations is reversed in Eq. (15) compared to Eq. (13); this is because the matrix  $G$  acts directly on the vector of fermionic creation operators in Eq. (14), and it should be placed at the right side of all matrices representing earlier rotations. To perform the transformation in Eq. (9), we require that the first  $N_f$  rows of  $U$  be equal to  $VQ$ ; see also Appendix A. With the example  $N = 6$  and  $N_f = 3$ , this condition is equivalent to

$$VQU^\dagger = \begin{pmatrix} 1 & 0 & 0 & 0 & 0 & 0 \\ 0 & 1 & 0 & 0 & 0 & 0 \\ 0 & 0 & 1 & 0 & 0 & 0 \end{pmatrix}. \quad (16)$$

A sequence of Givens rotations—acting on adjacent columns of  $VQ$  (corresponding to neighboring qubits in the JWT)—can achieve this as follows:

$$\begin{aligned} VQ &\rightarrow \begin{pmatrix} * & * & * & 0 & 0 & 0 \\ * & * & * & * & * & 0 \\ * & * & * & * & * & * \end{pmatrix} \rightarrow \begin{pmatrix} * & * & 0 & 0 & 0 & 0 \\ * & * & * & * & 0 & 0 \\ * & * & * & * & * & * \end{pmatrix} \\ &\rightarrow \begin{pmatrix} \lambda_1 & 0 & 0 & 0 & 0 & 0 \\ 0 & * & * & 0 & 0 & 0 \\ 0 & * & * & * & * & 0 \end{pmatrix} \rightarrow \begin{pmatrix} \lambda_1 & 0 & 0 & 0 & 0 & 0 \\ 0 & \lambda_2 & 0 & 0 & 0 & 0 \\ 0 & 0 & * & * & 0 & 0 \end{pmatrix} \\ &\rightarrow \begin{pmatrix} \lambda_1 & 0 & 0 & 0 & 0 & 0 \\ 0 & \lambda_2 & 0 & 0 & 0 & 0 \\ 0 & 0 & \lambda_3 & 0 & 0 & 0 \end{pmatrix} \rightarrow VQU^\dagger, \end{aligned} \quad (17)$$

where  $\lambda_j$ s are phase factors, i.e.,  $|\lambda_j| = 1$ . The red-colored matrix elements are zeroed out in each step; Givens rotations on nonoverlapping columns can be implemented in parallel [42]. The blue colored ones become zeros or phase factors automatically due to the orthonormality of the rows. The phase factors are brought to ones in the last step by single-qubit rotations; this step is unnecessary if the goal is to prepare a single Slater determinant. The total number of Givens rotations needed for the transformation  $U$  is

$$\begin{aligned} N_G &= NN_f - N_f(N_f - 1)/2 - N_f(N_f + 1)/2 \\ &= (N - N_f)N_f, \end{aligned} \quad (18)$$

and the circuit depth is  $N - 1$ . Our algorithm requires only  $N_f^2/4$  Givens rotations in the worst case, when  $N_f = N/2$ . In comparison, direct implementations without using the unitary freedom  $V$  double the number of Givens rotations to  $N_f^2/2$  [11, 42]. We also point out that the trick to reduce  $N_G$  by interchanging the roles of particles and holes [11] is no longer needed here, i.e., particles and holes are treated on an equal footing in our algorithm.

In summary, we have described a method to prepare a Slater determinant (7) using two-qubit gates that act only on neighboring qubits. Our method can be achieved in four steps:

1. Store the wavefunctions of the occupied orbitals in the rows of the matrix  $Q$ ,
2. Zero out the upper right matrix elements of  $Q$  using the freedom  $Q \rightarrow VQ$ ,
3. Diagonalize  $VQ$  using a sequence of Givens rotations as column transformations,
4. Find the quantum gates that correspond to the Givens rotations in step 3.

As mentioned above, this algorithm has been implemented as part of the open-source project OpenFermion [37]. The code takes as input the matrix  $Q$  from Eq. (7) describing a Slater determinant and outputs a sequence of elements of the form  $(j, k, \theta, \phi)$ , which describes a Givens rotation of columns  $j$  and  $k$ . Furthermore, rotations that can be performed in parallel are grouped together. We used the code to verify that the method described here does produce the desired Slater determinant.

#### IV. PREPARING FERMIONIC GAUSSIAN STATES

Fermionic Gaussian states [44, 45] can be regarded as a generalization of Slater determinants obtained by relaxing the constraint that the total number of particles be fixed. The celebrated BCS wavefunction [46] for superconductivity is a special case of fermionic Gaussian states. Verstraete *et al.* [36] demonstrated how to prepare the ground state of a BCS-like Hamiltonian—for 1D translationally invariant systems—using the fermionic fast Fourier transformation and the two-mode Bogoliubov transformation. Recently, superpositions of fermionic Gaussian states were used to approximate low energy states of quantum impurity models [47], which can be useful to a quantum-classical hybrid scheme for correlated materials [35]. Simulating quantum systems with disorder on a quantum computer may also lead to better understanding of and ultimately control over the emergent phases from impurities [30].

Here, we discuss how to prepare an arbitrary fermionic Gaussian state as the ground state of a quadratic Hamiltonian,

$$\mathcal{H} = \sum_{j,k=1}^N M_{jk} c_j^\dagger c_k + \frac{1}{2} \sum_{j,k=1}^N \left( \Delta_{jk} c_j^\dagger c_k^\dagger + \text{h.c.} \right), \quad (19)$$

where  $M = M^\dagger$  and  $\Delta = -\Delta^T$  are complex matrices. Python code for this algorithm is available as part of the OpenFermion project [37]. Our method can also be used to implement an arbitrary fermionic Gaussian unitary. In Appendix A, we review the standard approach to bring the Hamiltonian (19) into the diagonal form,

$$\mathcal{H} = \sum_{j=1}^N \varepsilon_j b_j^\dagger b_j + \text{c-number}, \quad (20)$$

where  $0 \leq \varepsilon_1 \leq \varepsilon_2 \leq \dots \leq \varepsilon_N$ , and  $b_j$  and  $b_j^\dagger$  are a new set of fermionic operators that satisfy the canonical anti-commutation relations. The new fermionic operators are linear combinations of the original ones:

$$\begin{pmatrix} \mathbf{b}^\dagger \\ \mathbf{b} \end{pmatrix} = W \begin{pmatrix} \mathbf{c}^\dagger \\ \mathbf{c} \end{pmatrix} = \begin{pmatrix} \mathcal{W} \mathbf{c}^\dagger \mathcal{W}^\dagger \\ \mathcal{W} \mathbf{c} \mathcal{W}^\dagger \end{pmatrix}, \quad (21)$$

where  $(\mathbf{c}^\dagger \ \mathbf{c})^T = (c_1^\dagger \dots c_N^\dagger \ c_1 \dots c_N)^T$  and  $(\mathbf{b}^\dagger \ \mathbf{b})^T = (b_1^\dagger \dots b_N^\dagger \ b_1 \dots b_N)^T$ . The fermionic Gaussian unitary  $\mathcal{W}$  performs the linear transformation  $W$ , and the ground state of the quadratic Hamiltonian (19) is

$$|\Psi_0\rangle = \mathcal{W} |\text{vac}\rangle = \mathcal{U} |\text{vac}\rangle, \quad (22)$$

where  $c_j |\text{vac}\rangle = 0$  for  $j = 1, 2, \dots, N$ , and  $\mathcal{U} = \mathcal{W}\mathcal{V}$  for some single-particle basis transformation  $\mathcal{V}$ . The unitary matrix  $W$  has the block form

$$W = \begin{pmatrix} W_1^* & W_2^* \\ W_2 & W_1 \end{pmatrix}, \quad (23)$$

where the submatrices satisfy

$$W_1 W_1^\dagger + W_2 W_2^\dagger = \mathbb{1}, \quad (24)$$

$$W_1 W_2^T + W_2 W_1^T = 0, \quad (25)$$

with  $\mathbb{1}$  and  $0$  being the  $N \times N$  identity matrix and zero matrix, respectively. We define the  $N \times 2N$  matrix  $W_L = (W_2 \ W_1)$  as the lower half of  $W$ ; the  $j$ th row of  $W_L$  corresponds to the expansion coefficients of the operator  $b_j$ . The matrix  $W_L$  uniquely determines the transformation  $\mathcal{W}$  up to an overall phase.

Using elementary matrix manipulations on  $W_L$ , we demonstrate that the Gaussian unitary  $\mathcal{U}$  in Eq. (22) can be broken into a sequence of operations that can be implemented on a quantum computer:

$$\mathcal{U} = \mathcal{B} \mathcal{G}_1 \mathcal{B} \mathcal{G}_2 \mathcal{G}_3 \mathcal{B} \dots \mathcal{G}_{N_G} \mathcal{B}, \quad (26)$$

where  $\mathcal{G}_j$ s are Givens rotations on adjacent fermionic modes encoded in the JWT and  $\mathcal{B} = c_N + c_N^\dagger$  denotes

the particle-hole Bogoliubov transformation on the last fermionic mode,

$$\mathcal{B}c_N\mathcal{B}^\dagger = c_N^\dagger, \quad (27)$$

$$\mathcal{B}c_j\mathcal{B}^\dagger = c_j, \text{ for } j = 1, 2, \dots, N-1. \quad (28)$$

The transformation  $\mathcal{B}$  does not conserve the total number of particles and is crucial to preparing superpositions of states with different numbers of particles. It can be implemented easily by applying the Pauli- $X$  operator on the last qubit; the parities of the other fermionic modes encoded in the JWT are not affected, which would not be true for any other spin orbital. In the relevant coordinate axes, the matrix representation of the Givens rotation is

$$G = \left( \begin{array}{cc|cc} \cos \theta & -e^{i\varphi} \sin \theta & 0 & 0 \\ \sin \theta & e^{i\varphi} \cos \theta & 0 & 0 \\ \hline 0 & 0 & \cos \theta & -e^{-i\varphi} \sin \theta \\ 0 & 0 & \sin \theta & e^{-i\varphi} \cos \theta \end{array} \right). \quad (29)$$

The representation of the particle-hole transformation is

$$B = B^\dagger = \begin{pmatrix} \mathbb{1} - e_N e_N^T & e_N e_N^T \\ e_N e_N^T & \mathbb{1} - e_N e_N^T \end{pmatrix}, \quad (30)$$

where  $e_N = (0, \dots, 0, 1)^T$  is an  $N$ -dimensional unit vector. The goal is to find a  $2N \times 2N$  unitary matrix  $U$

decomposed into  $G$  and  $B$ ,

$$U = B G_{N_G} \cdots B G_3 G_2 B G_1 B, \quad (31)$$

such that

$$V W_L U^\dagger = \left( \begin{array}{c|c} \mathbb{0} & \mathbb{1} \end{array} \right), \quad (32)$$

where  $V$  is an arbitrary unitary matrix. The right-hand side of Eq. (32) represents the original annihilation operators  $c_j$ , which corresponds to the vacuum state defined in Eq. (22). We discuss how to bring  $W_L$  to the desired form (32) using an example of four spin orbitals. Following Section III, we use the unitary  $V$  as a freedom to zero out some matrix elements on the left side of  $W_L$ ,

$$V W_L = \left( \begin{array}{cccc|cccc} 0 & 0 & 0 & * & * & * & * & 0 \\ 0 & 0 & * & * & * & * & * & * \\ 0 & * & * & * & * & * & * & * \\ * & * & * & * & * & * & * & * \end{array} \right), \quad (33)$$

where  $*$  represents an arbitrary matrix element and the blue colored matrix element is automatically zeroed out due to Eq. (25). A sequence of elementary operations that brings  $W_L$  to the desired form is

$$\begin{aligned} V W_L &\rightarrow \left( \begin{array}{cccc|cccc} 0 & 0 & 0 & 0 & * & * & * & * \\ 0 & 0 & * & * & * & * & * & * \\ 0 & * & * & * & * & * & * & * \\ * & * & * & * & * & * & * & * \end{array} \right) \rightarrow \left( \begin{array}{cccc|cccc} 0 & 0 & 0 & 0 & * & * & * & 0 \\ 0 & 0 & 0 & * & * & * & * & 0 \\ 0 & * & * & * & * & * & * & * \\ * & * & * & * & * & * & * & * \end{array} \right) \rightarrow \left( \begin{array}{cccc|cccc} 0 & 0 & 0 & 0 & * & * & 0 & 0 \\ 0 & 0 & 0 & 0 & * & * & * & * \\ 0 & 0 & 0 & 0 & * & * & * & * \\ * & 0 & * & * & * & * & * & * \end{array} \right) \rightarrow \left( \begin{array}{cccc|cccc} 0 & 0 & 0 & 0 & \lambda_1 & 0 & 0 & 0 \\ 0 & 0 & 0 & 0 & 0 & * & * & 0 \\ 0 & 0 & 0 & 0 & 0 & * & * & 0 \\ 0 & 0 & 0 & * & 0 & * & * & 0 \\ 0 & * & * & * & 0 & * & * & * \end{array} \right) \\ &\rightarrow \left( \begin{array}{cccc|cccc} 0 & 0 & 0 & 0 & \lambda_1 & 0 & 0 & 0 \\ 0 & 0 & 0 & 0 & 0 & \lambda_2 & 0 & 0 \\ 0 & 0 & 0 & 0 & 0 & 0 & * & * \\ 0 & 0 & 0 & 0 & 0 & 0 & * & * \\ 0 & 0 & * & * & 0 & 0 & * & * \end{array} \right) \rightarrow \left( \begin{array}{cccc|cccc} 0 & 0 & 0 & 0 & \lambda_1 & 0 & 0 & 0 \\ 0 & 0 & 0 & 0 & 0 & \lambda_2 & 0 & 0 \\ 0 & 0 & 0 & 0 & 0 & 0 & \lambda_3 & 0 \\ 0 & 0 & 0 & 0 & 0 & 0 & 0 & 0 \\ 0 & 0 & 0 & \lambda_4 & 0 & 0 & 0 & 0 \end{array} \right) \rightarrow V W_L U^\dagger. \quad (34) \end{aligned}$$

The red-colored matrix elements in the fourth column are always zeroed out by the particle-hole transformation  $B$ , and the other red-colored matrix elements on the left side are zeroed out by the Givens rotations  $G$ . The red-colored elements on the right side become nonzero due to the particle-hole transformation  $B$ , and the blue-colored matrix elements are brought to zeros or phase factors automatically by the condition (24) or (25). The phase factors are brought to ones in the last step by single-qubit rotations; this step is unnecessary if  $\mathcal{U}$  is applied to the vacuum state. The total numbers of Givens rotations

and particle-hole transformations are

$$N_G = (N-1)N/2, \quad N_B = N, \quad (35)$$

and the circuit depth is at most  $2N-1$ .

In summary, we have described a method to prepare an arbitrary Gaussian state as the ground state of the quadratic Hamiltonian (19) using two-qubit gates that act only on neighboring qubits. Our method can be achieved in four steps:

1. Calculate the matrix  $W$  using the procedure described in Appendix A,
2. Zero out the upper-left matrix elements of  $W_L$  using

the freedom  $W_L \rightarrow VW_L$  (33),

3. Zero out the remaining matrix elements on the left side of  $VW_L$  using the sequence (34),
4. Find the quantum gates corresponding to the sequence in step 3.

The procedure described here also applies to the implementation of an arbitrary Gaussian unitary, where one cannot use the unitary freedom  $V$ . By rearranging Eq. (32), we have

$$W_L = V^\dagger \begin{pmatrix} \mathbb{0} & \mathbb{1} \end{pmatrix} U = \begin{pmatrix} \mathbb{0} & \mathbb{1} \end{pmatrix} \begin{pmatrix} V^T & \mathbb{0} \\ \mathbb{0} & V^\dagger \end{pmatrix} U, \quad (36)$$

where the matrix  $\text{diag}(V^T, V^\dagger)$  corresponds to a basis change and can be decomposed as Givens rotations using the method discussed in Section III.

As mentioned above, this algorithm has also been implemented as part of OpenFermion [37]. The user can specify a quadratic Hamiltonian by inputting the matrices  $M$  and  $\Delta$  from Eq. (19). The code then outputs a sequence of operations, each of which describes either a Givens rotation or indicates a particle-hole transformation on the last fermionic mode. The operations that can be performed in parallel are grouped together. Since OpenFermion also contains modules to initialize common Hamiltonian models, it can be used to easily specify, for instance, a meanfield Hamiltonian, and then obtain a circuit that prepares its ground state. We used the code to verify that the method described here does produce the desired ground state.

## V. FERMIONIC FOURIER TRANSFORMATIONS

The fermionic Fourier transformation is a subroutine of many quantum algorithms. It was first introduced for quantum computing purposes in [36]. Recently, Babbush *et al.* [9] demonstrated that the 2D and 3D fermionic Fourier transformations can be implemented using a 2D qubit array with  $O(N)$  depth. Here, we present an algorithm to implement the 2D fermionic Fourier transformation using a 2D qubit array with only  $O(\sqrt{N})$  depth. This amount of depth is required for quantum information to travel across the array, and therefore this scaling is optimal. Our method provides an example where the parity problem in JWTs for more than one spatial dimension can be circumvented with negligible overhead. Our algorithm also works for more general transformations that can be factorized into a product of transforms on each spatial dimension, including Fourier transformations with open-boundary conditions and fermionic Gaussian unitaries. This algorithm allows one to efficiently prepare the initial states for systems whose ground states are well approximated by the meanfield states, as well as improve the efficiency of measurements.

In Section III, we have demonstrated that any fermionic single-particle basis transformation—including the 1D fermionic Fourier transformation—can be implemented using a 1D qubit chain with  $O(N^2)$  gates and  $O(N)$  depth; see also Theorem 7 in Ref. [9]. Using this algorithm as a subroutine, we discuss an algorithm that implements the 2D fermionic Fourier transformation using a 2D qubit array with  $O(N^{1.5})$  gates and  $O(\sqrt{N})$  depth. More generally, our method works for any fermionic single-particle basis transformation  $\mathcal{F}$  (or fermionic Gaussian unitary) that factorizes,

$$\mathcal{F} = \mathcal{F}_x \mathcal{F}_y = \mathcal{F}_y \mathcal{F}_x, \quad (37)$$

where the horizontal (vertical) transformation  $\mathcal{F}_x$  ( $\mathcal{F}_y$ ) is a product of commuting terms, each of which only involves spin orbitals in the same row (column). We map the fermionic operators to qubit operators using a snake-shaped JWT in row-major order; see Fig. 2. The trans-

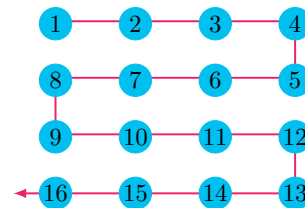


FIG. 2. The fermionic spin orbitals on a  $4 \times 4$  array are mapped to qubits (blue circles) on an array of the same dimensions using a snake-shaped JWT. The red arrow shows the direction of the JWT, and the qubits are numbered by their order in the JWT. Hopping terms between rows  $2n - 1$  and  $2n$  are called right-closed hopping terms, while those between rows  $2n$  and  $2n + 1$  are called left-closed hopping terms.

formation  $\mathcal{F}_x$  on a single row can be implemented with  $O(n_x^2)$  gates and  $O(n_x)$  depth using the algorithm described in Section III, where  $n_x$  is the number of spin orbitals in a single row (number of columns). The vertical transformation  $\mathcal{F}_y$  is much harder to implement because of the nonlocal parity operators in the hopping terms, see Eq. (5). This difficulty can be overcome by reordering the fermionic spin orbitals in the JWT using the fermionic SWAP gates; such a strategy allows one to perform the 2D fermionic Fourier transformation using a 2D qubit array with  $O(N^2)$  gates and  $O(N)$  depth [9]. We use a different approach that takes full advantage of the 2D qubit interactions. In our scheme, the transformation (37) is realized using the decomposition

$$\mathcal{F} = \mathcal{F}_x \mathcal{F}_y = \mathcal{F}_x \Gamma \mathcal{F}_y^\dagger \Gamma^\dagger, \quad (38)$$

where  $\Gamma$  is a diagonal unitary matrix with eigenvalues  $\pm 1$ . The unitary  $\mathcal{F}_y^\dagger$  is implemented by using Givens rotations without the parity operators attached; see Fig. 1. This is equivalent to using a JWT with column-major order, and the generators of the Givens rotations (without the

phase part) take the form (6a),

$$K_{jk} = \frac{1}{2}(X_j Y_k - Y_j X_k), \quad (39)$$

where the qubits  $j$  and  $k$  are adjacent in one column; we call these operators bare hopping terms. The unitary  $\mathcal{F}_y^b$  on a single column can be implemented with  $O(n_y^2)$  gates and  $O(n_y)$  depth using the bare hopping terms, where  $n_y$  is the number of spin orbitals per column. By parallelizing operations on different rows or columns of qubits, one can implement either  $\mathcal{F}_x$  or  $\mathcal{F}_y^b$  with  $O(N^{1.5})$  gates and  $O(\sqrt{N})$  depth, where  $N = n_x \times n_y$  is the number of spin orbitals. We will show that the unitary transformation  $\Gamma K_{jk} \Gamma^\dagger$  attaches the correct parity operators to the bare hopping terms  $K_{jk}$  for all  $j$  and  $k$  in the same column. Because  $\mathcal{F}_y$  can be decomposed into a product of Givens rotations generated by the vertical hopping terms with the parity operators attached, we have  $\Gamma \mathcal{F}_y^b \Gamma^\dagger = \mathcal{F}_y$ .

We show that the unitary  $\Gamma$  can be implemented with  $O(N)$  gates and  $O(\sqrt{N})$  circuit depth by introducing one ancillary qubit for each row. A schematic depiction of the quantum circuit for  $\Gamma$  is shown in Fig. 3. The ancilla

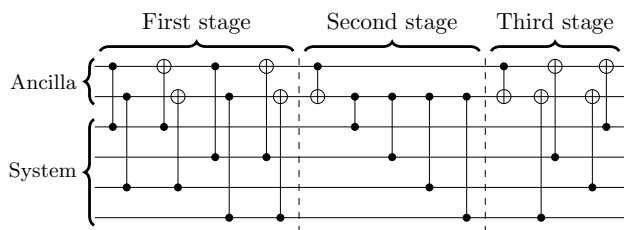


FIG. 3. Circuit implementation of  $\Gamma$  (for illustration purposes only). The CZ gates are used to attach the parities to the system qubits, and the CNOT gates are used to update the parities stored in the ancillary qubits.

qubits store the parities of the system qubits, which are updated using the controlled- $X$  (CNOT) gates. The ancillae are only used to facilitate the implementation of  $\Gamma$ ; they are disentangled with the system qubits in the end. The Pauli- $Z$  operator of an ancillary qubit  $a$  is attached to the Pauli- $X$  and  $Y$  operators of a system qubit  $s$  when a controlled- $Z$  (CZ) gate commutes through them as in Fig. 4; therefore, any hopping term that involves  $s$  picks up the parity stored in  $a$  in this process. After all the

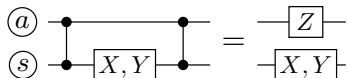


FIG. 4. The parity stored in the ancillary qubit  $a$  is attached to the Pauli- $X$  and  $-Y$  operators of the system qubit  $s$  when the CZ gate commutes through it.

gates in Fig. 3 have been commuted through the Pauli- $X$  or  $Y$  operator of  $s$ , it is attached with a string of Pauli- $Z$  operators of other system qubits. The unitary  $\Gamma$  can then

be combined with  $\Gamma^\dagger$  to identity. The goal is to attach all the bare vertical hopping terms on neighboring qubits with the correct parities; for example, the parity operator  $Z_2 Z_3 \cdots Z_7$  needs to be attached to the bare hopping term between qubits 1 and 8 in Fig. 2. We demonstrate how this is achieved by using two CZ gates in Fig. 5; the CNOT gate in Fig. 7a is neglected, because it is canceled by the corresponding CNOT gate in the third stage. Any non-neighboring vertical hopping terms can be de-

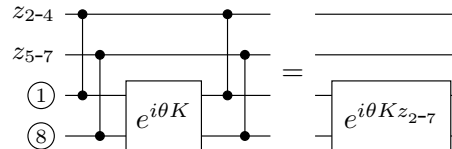


FIG. 5. The parities stored in the ancillae (two upper qubits) are attached to the bare hopping term  $K$  between qubits 1 and 8, where  $z_{j-k} = z_j z_{j+1} \cdots z_k$  denotes the value of the parity. The circuit identity in Fig. 4 is used twice to show the above circuit identity.

rived as (nested) commutators of the nearest-neighbor ones, and their parities are taken care of automatically. A Slater determinant in the momentum basis can thus be prepared by applying the transformation  $\mathcal{F}$  to a Slater determinant in the site basis  $|\Psi_S\rangle$ ,

$$\mathcal{F}|\Psi_S\rangle = \mathcal{F}_x \Gamma \mathcal{F}_y^b \Gamma^\dagger |\Psi_S\rangle = (-1)^\gamma \mathcal{F}_x \Gamma \mathcal{F}_y^b |\Psi_S\rangle, \quad (40)$$

where  $\gamma = \pm 1$  depends on the corresponding parity.

As depicted in Fig. 3, there are three stages in implementing  $\Gamma$ . We summarize them here using the example in Fig. 2 and describe in detail how they are achieved in the following paragraphs.

- In the first stage, the Pauli- $X$  or  $Y$  operator of a qubit is attached with the total parity of all the qubits to its right in the same row. For example,  $X_7$  is attached with  $Z_5 Z_6$ . This fixes the parities for any right-closed hopping term, e.g., the hopping term between qubits 2 and 7 is attached with  $Z_3 Z_4 Z_5 Z_6$ . However, the parities of the left-closed hopping terms are still incorrect, e.g., the hopping term between qubits 7 and 10 should be attached with  $Z_8 Z_9$ , not  $Z_5 Z_6 Z_{11} Z_{12}$ .
- In the second stage, the right-closed hopping terms are unchanged (up to a minus sign). Each left-closed hopping term is attached with the total parity of the two involved rows. This fixes the parities of the left-closed terms; for example, the hopping term between qubits 7 and 10 get the parity  $Z_5 Z_6 \cdots Z_{12}$  in this stage.
- In the third stage, the ancilla qubits are unentangled with the system qubits by applying the CNOT gates in the reversed order.

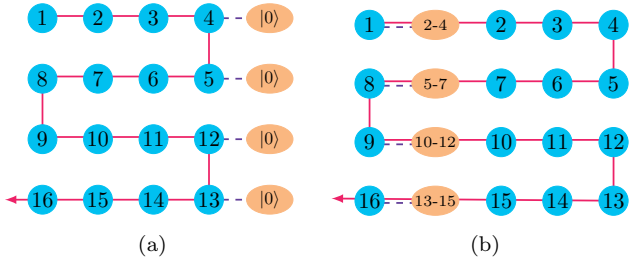


FIG. 6. First stage of implementing  $\Gamma$ . The orange ellipses represent the ancilla qubits used to store the parity of system qubits;  $j$ - $k$  indicates that the ancilla qubit stores the parity  $Z_{j-k} \equiv Z_j \cdots Z_k$ . The purple dashed lines represent quantum gates between qubits.

The first stage starts with the configuration in Fig. 6a with all the ancilla qubits set to the state  $|0\rangle$ . The ancilla qubits are then pushed to the left to interact with all the system qubits in the same row. The quantum gates between the ancilla qubits and the system qubits to the left are described in Fig. 7, where the CZ gate attaches

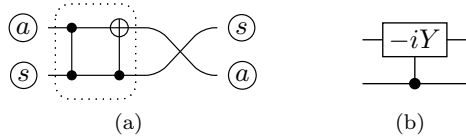


FIG. 7. Quantum circuit corresponding to Fig. 6: (a) the parity of the ancilla qubit  $a$  is attached to the system qubit  $s$  by the CZ gate, the parity stored in  $a$  is updated by the CNOT gate, and the qubits  $a$  and  $s$  are swapped, (b) an equivalent quantum gate to the part in the dotted box.

the parity stored in the ancilla qubit  $a$  to the system qubit  $s$ , the CNOT gate updates the parity stored in  $a$ , and the positions of  $a$  and  $s$  are exchanged by the SWAP gate. These steps are repeated until the ancilla qubits are pushed to the far left of the array (the first CZ gate and the last SWAP gate can be omitted). The first stage takes  $O(N)$  gates and  $O(\sqrt{N})$  depth to implement.

The second stage starts with the configuration in Fig. 8a, where each ancilla qubit stores the total parity of the system qubits in the same row; the vertical dashed line represents a CNOT gate which adds the parity stored in the ancilla in the third row to the one in the second row. In Fig 8b, the second ancilla is then swapped with system qubit 8. In Fig 8c, the two dashed lines represent the two CZ gates between the second ancilla and system qubits 1 and 8. This step affects the hopping terms between qubits 1 and 8 and qubits 8 and 9. The circuit identity in Fig. 4 cannot be used here directly because the hopping terms change the value of  $Z_8$  which is initially stored in the ancilla. We divide the parity stored in the ancilla into two parts: the part that involves the qubits in the hopping term, and the rest. The second part can be treated with the circuit identity in Fig. 4, while the

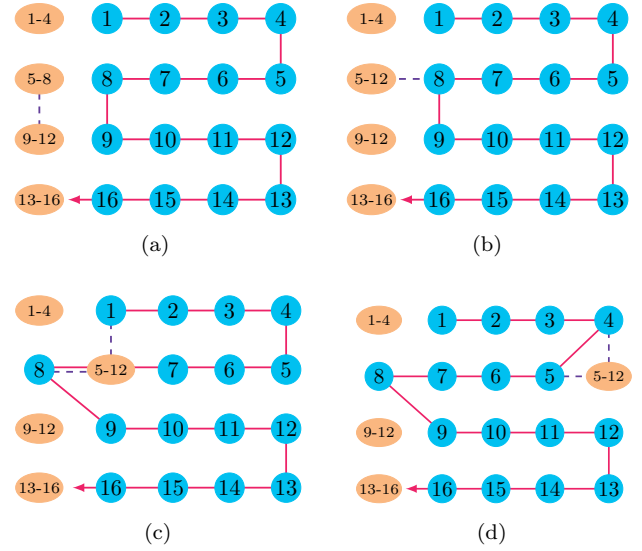


FIG. 8. Second stage of implementing  $\Gamma$ : the right-closed hopping terms are unchanged, while each left-closed hopping term is attached with the total parity of the qubits in the two involved rows.

first part requires more careful treatment. In Fig. 9, we retain the CNOT gates from the first and third stages corresponding to the system qubits involved in the hopping term. We use  $\bar{z}_{2-3}$  to denote the value of the product

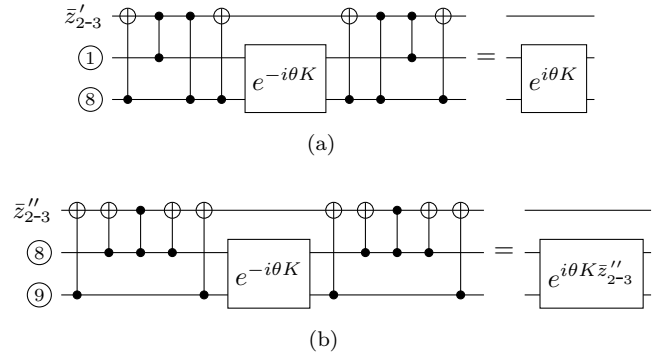


FIG. 9. The parities stored in the ancilla are attached to the Givens rotations in the second stage: (a) for the right-closed term between qubits 1 and 8 with  $\bar{z}'_{2-3} = \bar{z}_{2-3} z_8$ , (b) for the left-closed term between qubits 8 and 9 with  $\bar{z}''_{2-3} = \bar{z}_{2-3} z_8 z_9$ .

of all the Pauli- $Z$  operators on the second and third rows, e.g.,  $\bar{z}_{2-3} = z_5 z_6 \cdots z_{12}$ . The parity  $\bar{z}'_{2-3} = \bar{z}_{2-3} z_8$  excludes the contribution from qubit 8; after the first CNOT gate in Fig. 9a, the parity stored in the ancilla qubit is  $\bar{z}_{2-3}$ . Similarly, the parity  $\bar{z}''_{2-3} = \bar{z}_{2-3} z_8 z_9$  excludes the contributions from qubits 8 and 9; after the first two CNOT gates in Fig. 9b, the parity stored in the ancilla qubit is also  $\bar{z}_{2-3}$ . The commutation rules in Figs. 9a and 9b can be derived using the circuit identities in Figs. 10a and 10b, respectively. We also use the commutation relation  $[CZ, K] = 0$ , where the controlled- $Z$  operator and  $K$

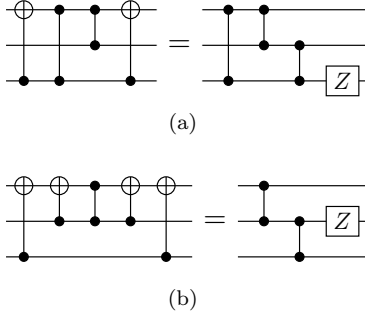


FIG. 10. Circuit identities used in Fig. 9.

act on the same pair of qubits. The extra minus signs in addition to the attached parities in Fig. 9 are due to the single Pauli- $Z$  operators in Fig. 10; they can be removed by reversing the sign of  $\theta$ . This step fixes the parity of the hopping term between qubits 8 and 9 without changing the parity of the hopping term between qubits 1 and 8. The second ancilla qubit is then pushed to the far right, and the corresponding gates are applied to each pair of system qubits and the ancilla; see Fig. 8d. Any hopping term between the first and second rows is unchanged in this process (up to a minus sign), while the hopping terms between the second and third rows pickup the total parity of the qubits on those two rows. This stage fixes the parity of the left-closed hopping terms.

The example of system size  $4 \times 4$  is too small to reveal some important ingredients in the second stage, especially the single CNOT gate in Fig. 8a. The quantum circuit for system size  $8 \times 8$  corresponding to the same step is shown in Fig. 11b, where  $\bar{z}_j$  denotes the total parity of the qubits on the  $j$ th row. This step is

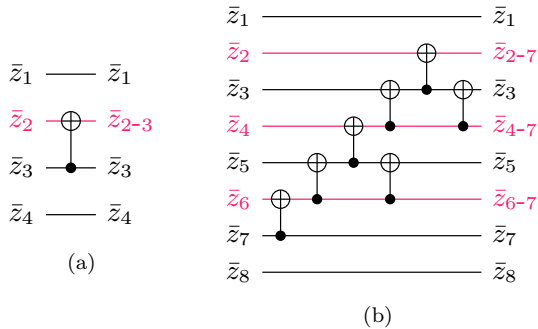


FIG. 11. Updating parities using neighboring CNOT gates: (a) circuit to perform the step 8a for a system of 4 rows, where  $\bar{z}_j$  denotes that the total parity of the  $j$ th row is stored in the corresponding ancilla qubit, (b) circuit to perform the same step for a system of 8 rows. The parities of the red-colored rows are being updated and are used in later steps.

needed because the parity of the ancilla qubit underneath a left-closed hopping term (except for the bottom ones) is also attached to this hopping term. In Fig. 12, we plot how the gates are commuted though the hopping term between qubits 16 and 24. The commutation relations

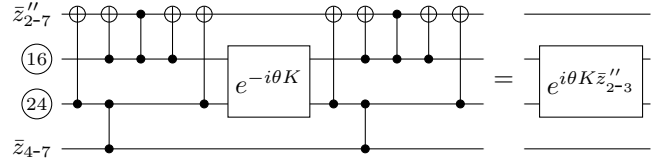


FIG. 12. Circuit identities for the left-closed term between qubits 16 and 24 in the  $8 \times 8$  system.

for the right-closed terms in the enlarged system are the same as the one described in Fig. 9a. Similarly, the parities of the left-closed hopping terms can be fixed without changing the right-closed terms. The step in Fig. 11 can be done with  $O(\sqrt{N})$  gates and  $O(\sqrt{N})$  depth; therefore, the second stage can be implemented with  $O(N)$  gates and  $O(\sqrt{N})$  depth. The third stage always takes less gates (no CZ gate) and depth to implement than the first two stages combined. Putting these results together, we conclude that  $\Gamma$  can be implemented with  $O(N)$  gates and  $O(\sqrt{N})$  depth.

The strategy described in this section is also useful for simulating the time evolution of fermionic systems, e.g., the Fermi-Hubbard model. In each Trotter step, the hopping terms can be implemented—using the help of  $\Gamma$ —with  $O(N)$  gates and  $O(\sqrt{N})$  depth.

## VI. THE FERMI-HUBBARD MODEL

One way to unravel the intricate physics in strongly correlated materials is to approximate them with idealized model Hamiltonians, such as the Fermi-Hubbard model. This model captures many signatures of the physical systems, although such a simple model cannot describe real materials quantitatively. The Hubbard model has resisted a full solution despite decades of intense analytical and numerical studies. It has a relatively small number of interacting terms, allowing for easy implementation on a quantum computer. The single-band Hubbard model is described by the Hamiltonian

$$\mathcal{H}_{\text{FH}} = - \sum_{\langle j,k \rangle, \sigma} t_{jk} (c_{j,\sigma}^\dagger c_{k,\sigma} + \text{h.c.}) + U \sum_j n_{j,\uparrow} n_{j,\downarrow} + \sum_{j,\sigma} (\epsilon_j - \mu) n_{j,\sigma} - \sum_j h_j (n_{j,\uparrow} - n_{j,\downarrow}), \quad (41)$$

where the first term represents fermions hopping between sites, the second term represents on-site interactions, the third term is a local potential field, and the last term represents a local magnetic field.

The 2D Hubbard model is widely used as a canonical microscopic model for strongly correlated fermionic systems. It is believed to be a key ingredient in understanding the mechanism behind high-temperature superconductivity [14]. In particular, understanding the physics of the model in the intermediate interaction strength regime

$U/t \sim 4$  in the underdoped region remains an open problem. Multiple orders exist in this region of its phase diagram, see Fig. 13. Even the nature of the ground

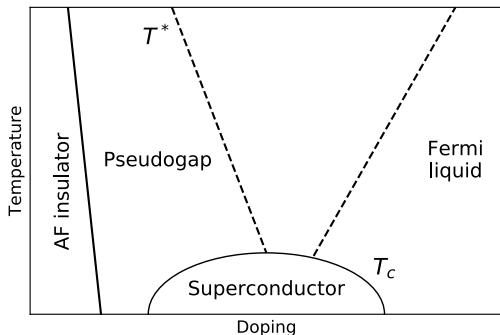


FIG. 13. Phase diagram of the 2D Fermi-Hubbard model: the critical temperature  $T_c$  depends on the value of hole doping, AF stands for Antiferromagnet and FL for Fermi liquid.

state remains ambiguous due to the competition between a number of different order parameters [48]. Significant progress has been made in the identification of the unconventional Mott-insulator transition and a superconducting phase with  $d$ -wave order parameter [49, 50]. Recently, the antiferromagnet phase of the Fermi-Hubbard model was realized in optical lattices of about 80 sites at a temperature of 1/4 times the tunnelling energy [29]. This region of multiple competing phases is also the most interesting regime from the point of view of modeling materials; therefore, a simulation using even a relatively small quantum computer could provide new qualitative and quantitative insights into the physics of the model [11, 51, 52]. Generalizations of the Hubbard model beyond the single band case and including more complicated lattices could be a route to modeling a wide range of strongly correlated materials. It is also a versatile tool for exploring strongly correlated electron phases [53] in a controlled way. Simulation of the Hubbard model on a quantum computer could allow quantitative analysis of the physical characteristics beyond the phase diagram, such as dynamical effects which could help uncover the deeper physics of the strongly correlated phases in the model.

In order to implement time evolution of the Hubbard model on a quantum computer, we decompose it into a product of available quantum gates based on the Trotter-Suzuki formula [54, 55]; the desired accuracy determines the number of time steps [56, 57]. We have simulated the Trotter error numerically for small system sizes in Appendix F. In each time step, we implement successively the horizontal hopping terms, the vertical hopping terms, and the remaining terms. The two spin states can be mapped to two sublattices of a 2D qubit array; for example, see Fig. 14. The horizontal hopping terms can be implemented by bringing qubits corresponding to the

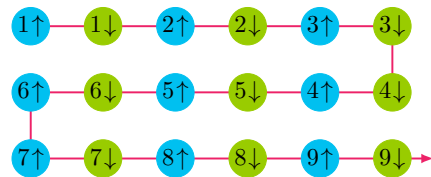


FIG. 14. One way to map the two spin states to qubits on a 2D qubit array using the JW method.

same spin states next to each other with the fermionic SWAP gates; for example, one can swap the qubits  $j \uparrow$  with  $j \downarrow$  for odd  $j$  in a row to implement some hopping terms, swap back, and then swap  $j \uparrow$  with  $j \downarrow$  for even  $j$  in the same row to implement the remaining hopping terms. This step requires  $O(N)$  gates and  $O(1)$  depth. The vertical hopping terms can be implemented using the method described in Section V; this requires  $O(N)$  gates and  $O(\sqrt{N})$  depth. Alternatively, the vertical hopping terms can be implemented using the method described in Appendix B also with  $O(N)$  gates and  $O(\sqrt{N})$  depth. The on-site interaction terms in Eq. (41) are mapped to qubit operators of the form,

$$n_{j\uparrow}n_{j\downarrow} \mapsto \frac{1}{4} (I - Z_{j\uparrow}) (I - Z_{j\downarrow}), \quad (42)$$

which can be implemented using a controlled-phase gate,

$$\exp(-i\tau U n_{j\uparrow}n_{j\downarrow}) \mapsto \begin{pmatrix} 1 & 0 & 0 & 0 \\ 0 & 1 & 0 & 0 \\ 0 & 0 & 1 & 0 \\ 0 & 0 & 0 & e^{-i\tau U} \end{pmatrix}. \quad (43)$$

The bias term and the magnetic term in the second line of Eq. (41) can be implemented straightforwardly with single-qubit operators. This step requires  $O(N)$  gates and  $O(1)$  depth. Putting all these steps together, each Trotter step can be simulated with only  $O(N)$  quantum gates and  $O(\sqrt{N})$  depth.

Cooper proved that an arbitrarily small attraction between electrons can cause pairing of electrons, leading to a lower energy state than the Fermi energy. As described in the BCS theory by Bardeen, Cooper, and Schrieffer [46], the  $s$ -wave pairing wavefunction due to electron-phonon interactions is responsible for conventional superconductivity. The cuprate superconductivity has  $d$ -wave symmetry [58, 59], wherein the superconducting wavefunction changes sign upon rotation by 90 degrees. It has been predicted that  $d$ -wave pairing underlies high- $T_c$  superconductivity in cuprates [60]; however, the mechanism of this pairing is not completely known. The mean-field Hamiltonian that describes  $d$ -wave pairing in the

single-band Hubbard model is

$$\begin{aligned} \mathcal{H}_{\text{DW}} = & - \sum_{\langle j,k \rangle, \sigma} t_{jk} \left( c_{j,\sigma}^\dagger c_{k,\sigma} + c_{k,\sigma}^\dagger c_{j,\sigma} \right) - \mu \sum_{j,\sigma} n_{j,\sigma} \\ & - \sum_{\langle j,k \rangle} \Delta_{jk}^{x^2-y^2} \left( c_{j\uparrow}^\dagger c_{k\downarrow}^\dagger - c_{j\downarrow}^\dagger c_{k\uparrow}^\dagger + \text{h.c.} \right), \end{aligned} \quad (44)$$

where the chemical potential term with  $\mu$  regulating the total number of particles, and  $\Delta_{jk}^{x^2-y^2} = \pm \Delta/2$  are the superconducting gaps for the horizontal and vertical directions, respectively. With the mapping in Fig. 14, the pairing term  $c_{j\uparrow}^\dagger c_{k\downarrow}^\dagger + \text{h.c.}$  can be implemented similarly to the hopping terms.

Assuming translational symmetry, the ground state of the Hamiltonian (44) can be prepared using the fermionic Fourier transformation,

$$c_{\mathbf{k},\sigma}^\dagger = \frac{1}{\sqrt{n_x n_y}} \sum_{j=1}^{n_x n_y} e^{2\pi i(k_x x_j + k_y y_j)} c_{j,\sigma}^\dagger, \quad (45)$$

where  $n_x$  ( $n_y$ ) is the number of sites in the horizontal (vertical) direction, and  $x_j \in \{1, \dots, n_x\}$  and  $y_j \in \{1, \dots, n_y\}$  denote the coordinates of the  $j$ th site. The discrete wavevector  $\mathbf{k} = (k_x, k_y)$  satisfies the condition  $k_x n_x \in \{1, \dots, n_x\}$  and similar for  $k_y$ . In the momentum basis, the Hamiltonian (44) becomes

$$\mathcal{H}_{\text{DW}} = \sum_{\mathbf{k},\sigma} \xi_{\mathbf{k}} c_{\mathbf{k},\sigma}^\dagger c_{\mathbf{k},\sigma} - \sum_{\mathbf{k}} \Delta_{\mathbf{k}} \left( c_{\mathbf{k}\uparrow}^\dagger c_{-\mathbf{k}\downarrow}^\dagger + \text{h.c.} \right), \quad (46)$$

where  $-\mathbf{k} \equiv (1 - k_x, 1 - k_y)$  and

$$\xi_{\mathbf{k}} = -2t \left( \cos(2\pi k_x) + \cos(2\pi k_y) \right) - \mu, \quad (47)$$

$$\Delta_{\mathbf{k}} = \Delta \left( \cos(2\pi k_x) - \cos(2\pi k_y) \right), \quad (48)$$

where  $\mu$  is chosen such that  $\xi_{\mathbf{k}} = 0$  at the Fermi surface. The BCS meanfield ground state of Eq. (46) is

$$|\Psi_{\text{DW}}\rangle = \prod_{\mathbf{k}} \left( u_{\mathbf{k}} + v_{\mathbf{k}} c_{\mathbf{k}\uparrow}^\dagger c_{-\mathbf{k}\downarrow}^\dagger \right) |\text{vac}\rangle, \quad (49)$$

$$u_{\mathbf{k}}^2 = \frac{1}{2} \left( 1 + \frac{\xi_{\mathbf{k}}}{\sqrt{\xi_{\mathbf{k}}^2 + |\Delta_{\mathbf{k}}|^2}} \right), \quad (50)$$

$$v_{\mathbf{k}}^2 = \frac{1}{2} \left( 1 - \frac{\xi_{\mathbf{k}}}{\sqrt{\xi_{\mathbf{k}}^2 + |\Delta_{\mathbf{k}}|^2}} \right), \quad (51)$$

where  $u_{\mathbf{k}} \geq 0$  and  $\text{sgn } v_{\mathbf{k}} = \text{sgn } \Delta_{\mathbf{k}}$ . Inspired by Ref. [36], we prepare the BCS ground state in the site basis by first preparing the ground state in the momentum basis (49) and then applying the 2D Fourier transformation to the two spin states, independently. The ground state in the momentum basis can be prepared by applying a Bogoliubov transformation to the vacuum state:

$$|\Psi_{\text{DW}}\rangle = \prod_{\mathbf{k}} \exp \left( \theta_{\mathbf{k}} c_{\mathbf{k}\uparrow}^\dagger c_{-\mathbf{k}\downarrow}^\dagger - \text{h.c.} \right) |\text{vac}\rangle, \quad (52)$$

where  $\sin \theta_{\mathbf{k}} = v_{\mathbf{k}}$ . The corresponding generator is

$$i \left( c_{\mathbf{k}\uparrow}^\dagger c_{-\mathbf{k}\downarrow}^\dagger - \text{h.c.} \right) \mapsto \frac{1}{2} \left( X_{\mathbf{k}\uparrow} Y_{-\mathbf{k}\downarrow} + Y_{\mathbf{k}\uparrow} X_{-\mathbf{k}\downarrow} \right), \quad (53)$$

where the qubit corresponding to the spin orbital  $-\mathbf{k}\downarrow$  is put right after that of  $\mathbf{k}\uparrow$  in the JWT. This unitary can be implemented with the quantum circuit in Fig. 15. The fermionic Fourier transformations can be performed

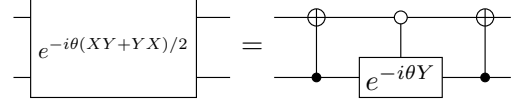


FIG. 15. Quantum circuit to implement the Bogoliubov transformation in the BCS state.

using the method described in Section V. The BCS meanfield state with periodic boundary conditions can thus be prepared using  $O(N^{1.5})$  gates and  $O(\sqrt{N})$  circuit depth.

In real experiments, it is often the case that open boundary conditions are used. In this case, the horizontal or vertical hopping terms in Eq. (44) correspond to a real triangular matrix with real eigenstates. We use these eigenstates as the single-particle basis states instead of the plane waves; therefore, the basis transformation matrix is also real. In the case of periodic boundary conditions, these real basis states correspond to

$$c_{\mathbf{k}+, \sigma}^\dagger = \frac{1}{\sqrt{2}} \left( c_{\mathbf{k}, \sigma}^\dagger + c_{-\mathbf{k}, \sigma}^\dagger \right), \quad (54)$$

$$c_{\mathbf{k}-, \sigma}^\dagger = \frac{-i}{\sqrt{2}} \left( c_{\mathbf{k}, \sigma}^\dagger - c_{-\mathbf{k}, \sigma}^\dagger \right). \quad (55)$$

for  $k_1, k_2 \leq 1/2$ . In this basis, the Hamiltonian (46) takes the form,

$$\begin{aligned} \mathcal{H}_{\text{DW}} = & \sum_{k_1, k_2 \leq 1/2, \sigma} \xi_{\mathbf{k}} \left( c_{\mathbf{k}+, \sigma}^\dagger c_{\mathbf{k}+, \sigma} + c_{\mathbf{k}-, \sigma}^\dagger c_{\mathbf{k}-, \sigma} \right) \\ & - \sum_{k_1, k_2 \leq 1/2} \Delta_{\mathbf{k}} \left( c_{\mathbf{k}+\uparrow}^\dagger c_{\mathbf{k}+\downarrow}^\dagger + c_{\mathbf{k}-\uparrow}^\dagger c_{\mathbf{k}-\downarrow}^\dagger + \text{h.c.} \right), \end{aligned} \quad (56)$$

where the pairing terms are also “diagonalized” as a consequence of the real transformation matrix. Therefore, one can prepare the meanfield ground state by first preparing the Bogoliubov ground state of the spin orbitals  $\mathbf{k}\pm\uparrow$  and  $\mathbf{k}\pm\downarrow$  before performing the real basis transformation. Similar to the case of periodic boundary conditions, the basis states on a 2D array with open boundary conditions can also be decomposed into a product of 1D basis states in each direction. This factorized form allows for efficient implementation of the 2D basis transformation with  $O(N^{1.5})$  gates and  $O(\sqrt{N})$  depth using the method described in Section V. When the Hamiltonian (44) does not satisfy translational symmetry, we can still prepare the meanfield ground state using the method described in Section IV. However, we might not be able to take advantage of the factorized form of

the transformation, and it takes  $O(N^2)$  gates and  $O(N)$  depth to prepare the meanfield ground state in the worst case.

The ground state of the 2D Fermi-Hubbard Hamiltonian (1) can be prepared by first preparing the meanfield ground state and then slowly interpolating from  $H_{\text{MF}}$  to  $H_{\text{FH}}$  [18]. Following Ref. [11], we introduce the Hamiltonian

$$\begin{aligned} \mathcal{H}(s) = & (1-s)\mathcal{H}_{\text{DW}} + s\mathcal{H}_{\text{FH}} \\ & - \zeta \sum_{\langle j,k \rangle} \Delta_{jk}^{x^2-y^2} \left( c_{j\uparrow}^\dagger c_{k\downarrow}^\dagger - c_{j\downarrow}^\dagger c_{k\uparrow}^\dagger \right) + \text{h.c.} \\ & - \eta \sum_{\langle\langle j,k \rangle\rangle} i\Delta_{jk}^{xy} \left( c_{j\uparrow}^\dagger c_{k\downarrow}^\dagger - c_{j\downarrow}^\dagger c_{k\uparrow}^\dagger \right) + \text{h.c.}, \end{aligned} \quad (57)$$

where  $s$  slowly changes from 0 to 1 in the adiabatic algorithm and  $\Delta_{jk}^{xy} = \Delta/2$  for  $x_j - x_k = \pm 1$  and  $y_j - y_k = \pm 1$ . The coefficients  $\zeta$  and  $\eta$  introduce small gaps to avoid quantum fluctuations of the  $d$ -wave order parameter and otherwise gapless nodal quasiparticles, respectively.

The initial Hamiltonian  $H_{\text{DW}}$  favors a meanfield ground state with  $d$ -wave symmetry of pairing order parameter. The algorithm proceeds in the following way. We initialize the system in a specific meanfield BCS-type wave function,

$$\mathcal{H}_{\text{MF}} | \Psi_{\text{MF}}(s=0) \rangle = E_0(s=0) | \Psi_{\text{MF}}(s=0) \rangle, \quad (58)$$

and adiabatically deform it to the ground state of the Hubbard model. If the initial wave function does not reflect the symmetry of the FH ground state, the adiabatic trajectory will encounter a quantum phase transition. This will manifest as a small spectral gap between the ground state and the excited states at the point of the transition, which vanishes in the thermodynamic limit. If the initial meanfield state reflects the symmetry of the ground state of the Hubbard model, there will be no phase transition and the spectral gap will remain independent of the system size in the course of the evolution. One indication that the phase transition occurred in the course of the evolution is the final state containing excitations above the pairing gap. This could be detected by measuring the average of the anomalous part of the Green's function. The controlled-phase gate (43) is implemented off-resonantly to achieve the required high fidelity. The optimal length of the gate translates into the limited strength of the effective interaction corresponding to roughly  $U \sim 10\text{MHz}$ . For the desired parameter regime  $U \sim 4t$ , an upper bound on the superconducting gap can be inferred from typical values of the order parameters obtained numerically,  $\Delta \lesssim 0.04t \sim 0.01U \sim 0.1\text{MHz}$ .

## VII. SUMMARY

In this paper we have discussed quantum simulation of strongly correlated fermionic systems using qubit arrays. We improved an existing quantum algorithm to

prepare an arbitrary Slater determinant [11, 42] by exploiting a unitary symmetry. We also presented a quantum algorithm to prepare an arbitrary fermionic Gaussian state with  $O(N^2)$  gates and  $O(N)$  circuit depth. This algorithm—unlike existing ones that rely on translational symmetry—is completely general and is useful for simulating disordered systems and quantum impurity models. Our quantum algorithms are optimal in the sense that the number of parameters in the quantum circuit is equal to that to describe the quantum states. We implemented these algorithms as a part of the open-source project OpenFermion [37].

We also presented an algorithm to implement the 2D fermionic Fourier transformation on a 2D qubit array with  $O(N^{1.5})$  gates and  $O(\sqrt{N})$  circuit depth, both of which scale better than methods based on fermionic SWAP gates [9]. A crucial step to achieve this optimal scaling is a unitary transformation that attaches the parity operators to the hopping terms; we show that it can be implemented with  $O(N)$  gates and  $O(\sqrt{N})$  circuit depth. This provides an example where the parity problem in simulating fermionic systems in more than one spatial dimension can be circumvented with almost no additional cost. Our algorithm can also be used for any 2D transformation that factorizes into horizontal and vertical terms, such as the fermionic Fourier transformation with open boundary conditions.

Using the Fermi-Hubbard model as an example, we discussed how to use our algorithms to find the ground state properties and phase diagrams of strongly correlated systems. We have demonstrated that the  $d$ -wave pairing meanfield states of the model can be prepared with  $O(N^{1.5})$  gates and  $O(\sqrt{N})$  depth. We have shown that each Trotter step in the time evolution can be implemented with  $O(N)$  gates and  $O(\sqrt{N})$  depth with only local qubit interactions. We discussed how to prepare the ground state of the model by adiabatically evolving the system from the meanfield Hamiltonian to the Hubbard Hamiltonian. The methods that we have developed can also be used for other quantum lattice models that suffer from the negative sign problem, e.g., frustrated spin systems, the  $t - J$  model, or lattice gauge theories.

In conclusion, we have shown that physical properties of strongly correlated fermionic systems can be simulated on available 2D qubit arrays with only  $O(N^{1.5})$  gates and  $O(\sqrt{N})$  circuit depth with very little overhead by using the Jordan-Wigner transformation. This result is one more step towards the goal of using quantum computers to investigate correlated quantum systems that are beyond the reach of any classical computer.

## VIII. ACKNOWLEDGMENTS

The authors would like to acknowledge enlightening and useful discussions with Ryan Babbush, Garnet Kin-Lic Chan, Chunjing Jia, Jarrod McClean, Andre Petukhov, Yaoyun Shi, Norman Tubman, and Fang

Zhang. This work is supported by the NASA Advanced Exploration Systems program and NASA Ames Research Center. The research is based in part upon work supported by the Office of the Director of National Intelligence (ODNI). The views and conclusions contained herein are those of the authors and should not be interpreted as necessarily representing the official policies or endorsements, either expressed or implied, of the ODNI or the U.S. Government. The U.S. Government is autho-

rized to reproduce and distribute reprints for Governmental purposes notwithstanding any copyright annotation thereon. K.J.S acknowledges support from NSF Grant No. 1717523. K.K. acknowledges support by NASA Academic Mission Services, contract number NNA16BD14C. All the quantum circuits in this work are plotted using the  $\langle q|pic$  system developed by Thomas Draper and Samuel Kutin.

- 
- [1] P. Hohenberg and W. Kohn, “Inhomogeneous Electron Gas,” *Physical Review* **136**, B864 (1964).
- [2] J. Quintanilla and C. Hooley, “The strong-correlations puzzle,” *Physics World* **22**, 32 (2009).
- [3] D. N. Basov, R. D. Averitt, D. van der Marel, M. Dressel, and K. Haule, “Electrodynamics of correlated electron materials,” *Reviews of Modern Physics* **83**, 471 (2011).
- [4] R. P. Feynman, “Simulating physics with computers,” *International Journal of Theoretical Physics* **21**, 467 (1982).
- [5] I. Georgescu, S. Ashhab, and F. Nori, “Quantum simulation,” *Reviews of Modern Physics* **86**, 153 (2014).
- [6] M. B. Hastings, D. Wecker, B. Bauer, and M. Troyer, “Improving Quantum Algorithms for Quantum Chemistry,” *Quantum Info. Comput.* **15**, 1 (2015).
- [7] A. Kandala, A. Mezzacapo, K. Temme, M. Takita, M. Brink, J. M. Chow, and J. M. Gambetta, “Hardware-efficient variational quantum eigensolver for small molecules and quantum magnets,” *Nature* **549**, 242 (2017).
- [8] M. Reiher, N. Wiebe, K. M. Svore, D. Wecker, and M. Troyer, “Elucidating reaction mechanisms on quantum computers,” *Proceedings of the National Academy of Sciences* **114**, 7555 (2017).
- [9] R. Babbush, N. Wiebe, J. McClean, J. McClain, H. Neven, and G. K.-L. Chan, “Low Depth Quantum Simulation of Electronic Structure,” [arXiv:1706.00023](https://arxiv.org/abs/1706.00023) (2017).
- [10] J. Hubbard, “Electron correlations in narrow energy bands,” *Proc. R. Soc. Lond. A* **276**, 238 (1963).
- [11] D. Wecker, M. B. Hastings, N. Wiebe, B. K. Clark, C. Nayak, and M. Troyer, “Solving strongly correlated electron models on a quantum computer,” *Physical Review A* **92**, 062318 (2015).
- [12] S. M. Griffin, P. Staar, T. C. Schulthess, M. Troyer, and N. A. Spaldin, “A bespoke single-band Hubbard model material,” *Phys. Rev. B* **93**, 075115 (2016).
- [13] M. S. Hybertsen, E. B. Stechel, M. Schluter, and D. R. Jennison, “Renormalization from density-functional theory to strong-coupling models for electronic states in Cu-O materials,” *Phys. Rev. B* **41**, 11068 (1990).
- [14] E. Dagotto, “Correlated electrons in high-temperature superconductors,” *Reviews of Modern Physics* **66**, 763 (1994).
- [15] E. H. Lieb and F. Y. Wu, “Absence of Mott transition in an exact solution of the short-range, one-band model in one dimension,” *Phys. Rev. Lett.* **20**, 1445 (1968).
- [16] T. Maier, M. Jarrell, T. Pruschke, and J. Keller, “*d*-wave superconductivity in the Hubbard model,” *Physical Review Letters* **85**, 1524 (2000).
- [17] B.-X. Zheng and G. K.-L. Chan, “Ground-state phase diagram of the square lattice Hubbard model from density matrix embedding theory,” *Physical Review B* **93**, 035126 (2016).
- [18] C. J. Jia, B. Moritz, C.-C. Chen, B. S. Shastry, and T. P. Devereaux, “Fidelity study of the superconducting phase diagram in the two-dimensional single-band Hubbard model,” *Phys. Rev. B* **84**, 125113 (2011).
- [19] S. Yamada, T. Imamura, and M. Machida, “16.447 tflops and 159-billion-dimensional exact-diagonalization for trapped fermion-hubbard model on the earth simulator,” in *Supercomputing, 2005. Proceedings of the ACM/IEEE SC 2005 Conference* (2005) pp. 44–44.
- [20] M. Troyer and U.-J. Wiese, “Computational Complexity and Fundamental Limitations to Fermionic Quantum Monte Carlo Simulations,” *Physical Review Letters* **94**, 170201 (2005).
- [21] S. R. White, “Density-matrix algorithms for quantum renormalization groups,” *Physical Review B* **48**, 10345 (1993).
- [22] M. H. Hettler, M. Mukherjee, M. Jarrell, and H. R. Krishnamurthy, “Dynamical cluster approximation: Non-local dynamics of correlated electron systems,” *Physical Review B* **61**, 12739 (2000).
- [23] G. Kotliar, S. Y. Savrasov, K. Haule, V. S. Oudovenko, O. Parcollet, and C. A. Marianetti, “Electronic structure calculations with dynamical mean-field theory,” *Reviews of Modern Physics* **78**, 865 (2006).
- [24] G. Knizia and G. K.-L. Chan, “Density Matrix Embedding: A Simple Alternative to Dynamical Mean-Field Theory,” *Physical Review Letters* **109**, 186404 (2012).
- [25] G. Ortiz, J. E. Gubernatis, E. Knill, and R. Laflamme, “Quantum algorithms for fermionic simulations,” *Physical Review A* **64**, 022319 (2001).
- [26] J. D. Whitfield, J. Biamonte, and A. Aspuru-Guzik, “Simulation of electronic structure Hamiltonians using quantum computers,” *Molecular Physics* **109**, 735 (2011).
- [27] A. A. Houck, H. E. Türeci, and J. Koch, “On-chip quantum simulation with superconducting circuits,” *Nature Physics* **8**, 292 (2012).
- [28] R. Barends, A. Shabani, L. Lamata, J. Kelly, A. Mezzacapo, U. L. Heras, R. Babbush, A. G. Fowler, B. Campbell, Y. Chen, Z. Chen, B. Chiaro, A. Dunsworth, E. Jeffrey, E. Lucero, A. Megrant, J. Y. Mutus, M. Neeley, C. Neill, P. J. J. O’Malley, C. Quintana, P. Roushan, D. Sank, A. Vainsencher, J. Wenner, T. C. White, E. Solano, H. Neven, and J. M. Martinis, “Digitized adi-

- abatic quantum computing with a superconducting circuit,” *Nature* **534**, 222 (2016).
- [29] A. Mazurenko, C. S. Chiu, G. Ji, M. F. Parsons, M. Kanász-Nagy, R. Schmidt, F. Grusdt, E. Demler, D. Greif, and M. Greiner, “A cold-atom Fermi-Hubbard antiferromagnet,” *Nature* **545**, 462 (2017).
- [30] S. Seo, X. Lu, J.-X. Zhu, R. R. Urbano, N. Curro, E. D. Bauer, V. A. Sidorov, L. D. Pham, T. Park, Z. Fisk, and J. D. Thompson, “Disorder in quantum critical superconductors,” *Nature Physics* **10**, 120 (2013).
- [31] B. Sacépé, T. Dubouchet, C. Chapelier, M. Sanquer, M. Ovadia, D. Shahar, M. Feigel’man, and L. Ioffe, “Localization of preformed Cooper pairs in disordered superconductors,” *Nature Physics* **7**, 239 (2011).
- [32] S. Kondov, W. McGehee, W. Xu, and B. DeMarco, “Disorder-Induced Localization in a Strongly Correlated Atomic Hubbard Gas,” *Physical Review Letters* **114**, 083002 (2015).
- [33] J.-X. Zhu, I. Martin, and A. R. Bishop, “Spin and Charge Order around Vortices and Impurities in High- $T_c$  Superconductors,” *Physical Review Letters* **89**, 067003 (2002).
- [34] B. M. Andersen, P. J. Hirschfeld, A. P. Kampf, and M. Schmid, “Disorder-Induced Static Antiferromagnetism in Cuprate Superconductors,” *Physical Review Letters* **99**, 147002 (2007).
- [35] B. Bauer, D. Wecker, A. J. Millis, M. B. Hastings, and M. Troyer, “Hybrid Quantum-Classical Approach to Correlated Materials,” *Physical Review X* **6**, 031045 (2016).
- [36] F. Verstraete, J. I. Cirac, and J. I. Latorre, “Quantum circuits for strongly correlated quantum systems,” *Physical Review A* **79**, 032316 (2009).
- [37] J. R. McClean, I. D. Kivlichan, D. S. Steiger, Y. Cao, E. S. Fried, C. Gidney, T. Häner, V. Havlíček, Z. Jiang, M. Neeley, J. Romero, N. Rubin, N. P. D. Sawaya, K. Setia, S. Sim, W. Sun, K. Sung, and R. Babbush, “OpenFermion: The electronic structure package for quantum computers,” [arXiv:1710.07629](https://arxiv.org/abs/1710.07629) (2017).
- [38] B. P. Lanyon, J. D. Whitfield, G. G. Gillett, M. E. Goggin, M. P. Almeida, I. Kassal, J. D. Biamonte, M. Mohseni, B. J. Powell, M. Barbieri, A. Aspuru-Guzik, and A. G. White, “Towards quantum chemistry on a quantum computer,” *Nature Chemistry* **2**, 106 (2010).
- [39] S. B. Bravyi and A. Y. Kitaev, “Fermionic Quantum Computation,” *Annals of Physics* **298**, 210 (2002).
- [40] J. T. Seeley, M. J. Richard, and P. J. Love, “The Bravyi-Kitaev transformation for quantum computation of electronic structure,” *The Journal of Chemical Physics* **137**, 224109 (2012).
- [41] F. Verstraete and J. I. Cirac, “Mapping local Hamiltonians of fermions to local Hamiltonians of spins,” *Journal of Statistical Mechanics: Theory and Experiment* **2005**, P09012 (2005).
- [42] I. D. Kivlichan, J. McClean, N. Wiebe, C. Gidney, A. Aspuru-Guzik, G. K.-L. Chan, and R. Babbush, “Quantum simulation of electronic structure with linear depth and connectivity,” [arXiv:1711.04789](https://arxiv.org/abs/1711.04789) (2017).
- [43] G. Wendin, “Quantum information processing with superconducting circuits: a review,” *Reports on Progress in Physics* **80**, 106001 (2017).
- [44] V. Bach, E. H. Lieb, and J. P. Solovej, “Generalized Hartree-Fock theory and the Hubbard model,” *Journal of Statistical Physics* **76**, 3 (1994).
- [45] E. Greplová, *Quantum Information with Fermionic Gaussian States*, Master’s thesis, LMU, München (2013).
- [46] J. Bardeen, L. N. Cooper, and J. R. Schrieffer, “Microscopic Theory of Superconductivity,” *Physical Review* **106**, 162 (1957).
- [47] S. Bravyi and D. Gosset, “Complexity of Quantum Impurity Problems,” *Communications in Mathematical Physics* **356**, 451 (2017).
- [48] B.-X. Zheng, C.-M. Chung, P. Corboz, G. Ehlers, M.-P. Qin, R. M. Noack, H. Shi, S. R. White, S. Zhang, and G. K.-L. Chan, “Stripe order in the underdoped region of the two-dimensional Hubbard model,” [arXiv:1701.00054](https://arxiv.org/abs/1701.00054) (2016).
- [49] C. J. Halboth and W. Metzner, “Renormalization-group analysis of the two-dimensional Hubbard model,” *Physical Review B* **61**, 7364 (2000).
- [50] T. A. Maier, M. Jarrell, T. C. Schulthess, P. R. C. Kent, and J. B. White, “Systematic study of  $d$ -wave superconductivity in the 2D repulsive hubbard model,” *Physical Review Letters* **95**, 237001 (2005).
- [51] D. S. Abrams and S. Lloyd, “Simulation of many-body Fermi systems on a universal quantum computer,” *Phys. Rev. Lett.* **79**, 2586 (1997).
- [52] D. S. Abrams and S. Lloyd, “Quantum algorithm providing exponential speed increase for finding eigenvalues and eigenvectors,” *Phys. Rev. Lett.* **83**, 5162 (1999).
- [53] S. Sachdev, “The landscape of the Hubbard model,” in *String Theory and Its Applications* (World Scientific, 2012) pp. 559–620.
- [54] H. F. Trotter, “On the product of semi-groups of operators,” *Proceedings of the American Mathematical Society* **10**, 545 (1959).
- [55] M. Suzuki, “Generalized Trotter’s formula and systematic approximants of exponential operators and inner derivations with applications to many-body problems,” *Communications in Mathematical Physics* **51**, 183 (1976).
- [56] R. Babbush, J. McClean, D. Wecker, A. Aspuru-Guzik, and N. Wiebe, “Chemical basis of Trotter-Suzuki errors in quantum chemistry simulation,” *Physical Review A* **91**, 022311 (2015).
- [57] D. Poulin, M. B. Hastings, D. Wecker, N. Wiebe, A. C. Doherty, and M. Troyer, “The Trotter Step Size Required for Accurate Quantum Simulation of Quantum Chemistry,” *Quantum Info. Comput.* **15**, 361 (2015).
- [58] D. A. Wollman, D. J. Van Harlingen, W. C. Lee, D. M. Ginsberg, and A. J. Leggett, “Experimental determination of the superconducting pairing state in YBCO from the phase coherence of YBCO-Pb dc SQUIDS,” *Physical Review Letters* **71**, 2134 (1993).
- [59] C. C. Tsuei and J. R. Kirtley, “Pairing symmetry in cuprate superconductors,” *Reviews of Modern Physics* **72**, 969 (2000).
- [60] D. J. Scalapino, “The case for  $d_{x^2-y^2}$  pairing in the cuprate superconductors,” *Physics Reports* **250**, 329 (1995).
- [61] J. Werschnik and E. K. U. Gross, “Quantum Optimal Control Theory,” [arXiv:0707.1883](https://arxiv.org/abs/0707.1883) (2007).
- [62] J.-M. Reiner, M. Marthaler, J. Braumüller, M. Weides, and G. Schön, “Emulating the one-dimensional Fermi-Hubbard model by a double chain of qubits,” *Physical Review A* **94**, 032338 (2016).
- [63] J. R. Johansson, P. D. Nation, and F. Nori, “QuTiP 2: A Python framework for the dynamics of open quantum

systems," *Computer Physics Communications* **184**, 1234 (2013).

### Appendix A: Quadratic Hamiltonians

Hamiltonians that are quadratic in fermionic creation and annihilation operators are important in the mean-field descriptions of many-body quantum systems. The most general form of a quadratic Hamiltonian is

$$\mathcal{H} = \sum_{j,k=1}^N (M_{jk} - \mu\delta_{jk}) c_j^\dagger c_k + \frac{1}{2} \sum_{j,k=1}^N (\Delta_{jk} c_j^\dagger c_k^\dagger + \text{h.c.}), \quad (\text{A1})$$

where  $M = M^\dagger$  and  $\Delta = -\Delta^T$  are complex matrices, and the chemical potential  $\mu$  regulates the total number of particles; hereafter,  $\mu$  will be absorbed into  $M$  to simplify notations. We review the standard results on how to bring  $\mathcal{H}$  into the diagonal form,

$$\mathcal{H} = \sum_{j=1}^N \varepsilon_j b_j^\dagger b_j + \text{c-number}, \quad (\text{A2})$$

where  $b_j$  and  $b_j^\dagger$  are a new set of fermionic operators that satisfy the canonical anticommutation relations.

When the number of particles is conserved ( $\Delta = 0$ ), the Hamiltonian (A1) takes the form

$$\mathcal{H} = \sum_{j,k=1}^N M_{jk} c_j^\dagger c_k. \quad (\text{A3})$$

The commutator of  $\mathcal{H}$  and a single creation operator is

$$\begin{aligned} [\mathcal{H}, c_l^\dagger] &= \sum_{jk} M_{jk} [c_j^\dagger c_k, c_l^\dagger] \\ &= \sum_{jk} M_{jk} c_j^\dagger \delta_{kl} = \sum_j M_{jl} c_j^\dagger. \end{aligned} \quad (\text{A4})$$

In matrix form, we have

$$[\mathcal{H}, \mathbf{c}^\dagger] = M^T \mathbf{c}^\dagger = M^* \mathbf{c}^\dagger, \quad (\text{A5})$$

where  $\mathbf{c}^\dagger = (c_1^\dagger \cdots c_N^\dagger)^T$ . The time evolution under the Hamiltonian  $\mathcal{H}$  takes the form,

$$e^{-i\tau\mathcal{H}} \mathbf{c}^\dagger e^{i\tau\mathcal{H}} = e^{-i\tau M^T} \mathbf{c}^\dagger. \quad (\text{A6})$$

Therefore, the time evolution of the  $2^N \times 2^N$  matrix  $\mathcal{H}$  can be represented by the  $N \times N$  unitary matrix  $e^{-i\tau M^T}$ . The quadratic form (A3) can be diagonalized into the form (A2) by introducing the fermionic operators  $b_j$  and  $b_j^\dagger$  such that

$$\mathbf{b}^\dagger = U \mathbf{c}^\dagger, \quad U M^T U^\dagger = \text{diag}(\varepsilon_1, \dots, \varepsilon_N), \quad (\text{A7})$$

where  $U$  is an  $N \times N$  unitary matrix, and the eigenvalues satisfy  $\varepsilon_1 \leq \varepsilon_2 \cdots \leq \varepsilon_N$ . In the  $N_f$ -particle sector, the ground state of the Hamiltonian (A3) corresponds to a Slater determinant with the  $Q$  matrix being the first  $N_f$  rows of  $U$ , see Eq. (7).

When the number of particles is not conserved, we rewrite the Hamiltonian (A1) in matrix form,

$$\mathcal{H} = \frac{1}{2} \begin{pmatrix} \mathbf{c}^\dagger & \mathbf{c} \end{pmatrix} \begin{pmatrix} \Delta & M \\ -M^* & -\Delta^* \end{pmatrix} \begin{pmatrix} \mathbf{c}^\dagger \\ \mathbf{c} \end{pmatrix} + \text{c-number}, \quad (\text{A8})$$

where the extra constant comes from different ordering of the fermionic operators; the matrix form (A8) is symmetrically ordered, while the form in Eq. (A1) is normal-ordered. The standard way to diagonalize the Hamiltonian (A8) is by solving the Bogoliubov de Gennes equations, which is somewhat cumbersome for numerical implementations. Alternatively, one introduces the Majorana fermion operators,

$$f_j = \frac{1}{\sqrt{2}}(c_j^\dagger + c_j), \quad f_{j+N} = \frac{i}{\sqrt{2}}(c_j^\dagger - c_j), \quad (\text{A9})$$

for  $j = 1, 2, \dots, N$ , which satisfy the anticommutation relations

$$\{f_j, f_k\} = \delta_{jk}, \quad \text{for } j, k = 1, 2, \dots, 2N. \quad (\text{A10})$$

In matrix form, the transformation (A9) reads

$$\mathbf{f} = \Omega \begin{pmatrix} \mathbf{c}^\dagger \\ \mathbf{c} \end{pmatrix}, \quad \Omega = \frac{1}{\sqrt{2}} \begin{pmatrix} \mathbb{1} & \mathbb{1} \\ i\mathbb{1} & -i\mathbb{1} \end{pmatrix}, \quad (\text{A11})$$

where  $\mathbf{f} = (f_1 \ f_2 \ \cdots \ f_{2N})^T$ . The Hamiltonian (A8) can be rewritten in terms of the Majorana fermion operators:

$$\mathcal{H} = \frac{i}{2} \mathbf{f}^T A \mathbf{f} + \text{c-number}, \quad (\text{A12})$$

where  $A$  is a  $2N \times 2N$  real antisymmetric matrix,

$$A = -i\Omega^* \begin{pmatrix} \Delta & M \\ -M^* & -\Delta^* \end{pmatrix} \Omega^\dagger. \quad (\text{A13})$$

Conversely, any real antisymmetric matrix  $A$  corresponds to a quadratic Hamiltonian of the form (A1). The commutator between a single Majorana fermion and the Hamiltonian  $\mathcal{H}$  is

$$[\mathcal{H}, f_l] = \frac{i}{2} \sum_{j \neq k} A_{jk} [f_j f_k, f_l] = i \sum_{j \neq l} A_{jl} f_j. \quad (\text{A14})$$

Using the matrix form  $[\mathcal{H}, \mathbf{f}] = -iA\mathbf{f}$ , we have

$$e^{-i\tau\mathcal{H}} \mathbf{f} e^{i\tau\mathcal{H}} = e^{-\tau A} \mathbf{f}. \quad (\text{A15})$$

Therefore, the unitary evolution of the Hamiltonian  $\mathcal{H}$  can be represented by the orthogonal matrix  $e^{-\tau A}$ . The

matrix  $A$  can be brought into the standard form (equivalent to the Schur form up to a permutation) by an orthogonal transformation  $R$ ,

$$RAR^T = \begin{pmatrix} 0 & \mathcal{E} \\ -\mathcal{E} & 0 \end{pmatrix}, \quad \mathcal{E} = \text{diag}(\varepsilon_1, \dots, \varepsilon_N), \quad (\text{A16})$$

where  $0 \leq \varepsilon_1 \leq \varepsilon_2 \leq \dots \leq \varepsilon_N$ . This transformation corresponds to a basis change of the Majorana fermions  $\mathbf{f}' = R\mathbf{f}$ , where the new operators  $\mathbf{f}'$  also satisfy the anticommutation relations (A10). Going back to the picture of creation and annihilation operators, such a basis transformation takes the form,

$$\begin{pmatrix} \mathbf{b}^\dagger \\ \mathbf{b} \end{pmatrix} = W \begin{pmatrix} \mathbf{c}^\dagger \\ \mathbf{c} \end{pmatrix}, \quad (\text{A17})$$

where  $(\mathbf{b}^\dagger \ \mathbf{b})^T = (b_1^\dagger \dots b_N^\dagger \ b_1 \dots b_N)^T$  and  $(\mathbf{c}^\dagger \ \mathbf{c})^T = (c_1^\dagger \dots c_N^\dagger \ c_1 \dots c_N)^T$ . The unitary matrix  $W$  defines a new set of fermionic operators  $b_j$  and  $b_j^\dagger$  which brings the Hamiltonian (A1) to the diagonal form (A2). The matrix  $W$  is related to  $R$  through a basis transformation,

$$W = \Omega^\dagger R \Omega. \quad (\text{A18})$$

It is the starting point of our procedure in Section IV, which prepares the ground state of the Hamiltonian (A1) on a quantum computer. In summary,  $W$  can be calculated in four steps:

1. Write the quadratic Hamiltonian (A1) into the matrix form (A8),
2. Find the real antisymmetric matrix  $A$  using the matrix form (A8) and Eq. (A13),
3. Bring  $A$  into the standard form (A16) using an orthogonal transformation  $R$ ,
4. Calculate the matrix  $W$  using  $R$  and Eq. (A18).

### Appendix B: Ancilla-assisted fermionic gates

In Section V, we discussed how to implement the 2D fermionic Fourier transformation with  $O(N^{1.5})$  gates and  $O(\sqrt{N})$  circuit depth. A crucial ingredient of our method is a unitary that attaches the corresponding parity operators to the bare hopping terms. This allows efficient implementation of both horizontal and vertical hopping terms on a 2D qubit array. The same strategy can be used to simulate Hamiltonian time evolution—again on a 2D qubit array—by Trotterization, where a single time step can be achieved with only  $O(N)$  gates and  $O(\sqrt{N})$  depth. Here, we propose an alternative method to implement the hopping terms in a Trotter step using ancilla qubits to store the parities also with  $O(N)$  gates and  $O(\sqrt{N})$  depth. However, it is less efficient in circuit

depth to perform the 2D Fourier transformation compared to the method in Section V due to difficulties in parallelization.

We discuss how to implement the hopping terms on a 2D qubit array using the same example of array size  $4 \times 4$ . The ancilla qubits move horizontally in the array to facilitate vertical hopping terms; see Fig. 16. The ancilla

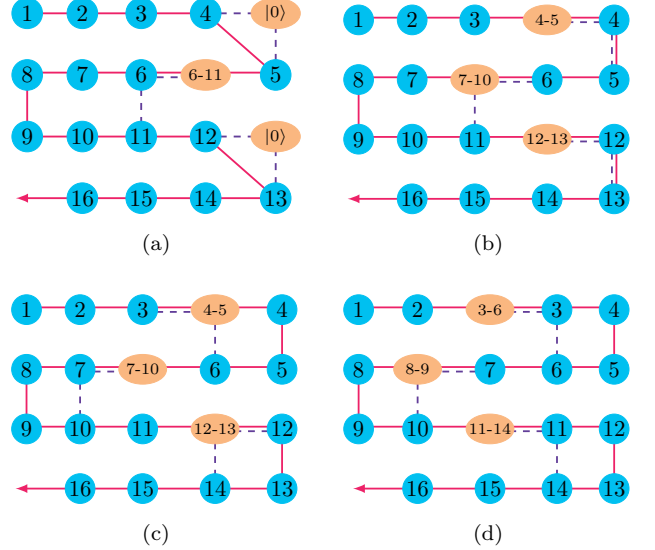


FIG. 16. Implementing the hopping terms on a  $4 \times 4$  qubit array. The red arrow indicates the direction of the JWT and the system qubits (blue circles) are numbered by their order in the JWT. The ancilla qubits (orange ellipses) store the parity information of the system qubits, where  $j-k$  denotes the parity  $Z_{j-k} \equiv Z_j \dots Z_k$ . The purple dashed lines represent quantum gates between neighboring qubits.

qubits are initially at the far left side of the qubit array; the states of those ancilla qubits for the right-closed hopping terms are set to  $|0\rangle$ , while those for the left-closed hopping terms store the parities of the two corresponding rows, e.g., the ancilla on the second row initially stores the parity  $Z_{5-12}$ . The vertical hopping terms are implemented with the parity stored in the ancilla qubits, whose states are updated constantly. For example, the vertical hopping term between qubits 3 and 6 in Fig. 16d is

$$\tilde{K}_{3,6} Z_{4-5} = -\tilde{K}_{3,6} Z_{3-6}, \quad (\text{B1})$$

where  $\tilde{K}_{3,6} = (X_3 X_6 + Y_3 Y_6)/2$  denotes the bare hopping term. The time evolution  $\exp(-i\tau \tilde{K}_{3,6})$  can be implemented using the second part of the circuit in Fig. 17, where the parity stored in the ancilla qubit is attached to the bare hopping term  $\tilde{K}_{3,6}$  by the CZ gates; the first part of the circuit, corresponding to Fig. 16c, updates the parity and swaps the ancilla qubit with system qubit 3. The order of the two parts in Fig. 17 may be reversed for other hopping terms, e.g., the one between system qubits 7 and 10; see Figs. 16c and 16d. After the ancilla qubits have swept over the entire rows, they are pushed back in

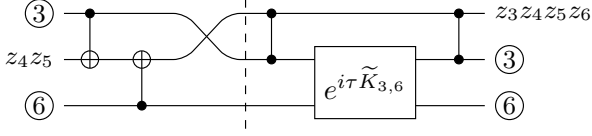


FIG. 17. Quantum circuit to implement the vertical hopping term between qubits 3 and 6.

the reverse direction and the same procedure starts over again. The vertical hopping terms require  $O(N)$  two-qubit gates to implement for a single Trotter step. The horizontal hopping terms can be implemented straightforwardly as long as the two involved qubits are at the same side of the ancilla qubit (no need to update the parity).

In Appendix E, we discuss how to simulate the 2D Fermi-Hubbard model with qubits on a ladder, i.e., two coupled chains. The basic idea is to use the fermionic SWAP gate to change between the row-major order and the column-major order, so that both the horizontal and vertical couplings can be implemented with only local interactions. This idea has also been proposed by Kivlichan *et al.* [42], independently. Because such a strategy does not take full advantage of the 2D qubit interactions, the number of gates scales as  $O(N^{1.5})$  which is worse than  $O(N)$  by using the methods described above and in Section V.

### Appendix C: Hamiltonian-based fermionic gates

Using methods in quantum optimal control [61], one can prepare desired quantum states by applying sequences of Hamiltonian evolutions to initial states that are easy to prepare. When the fermionic Hamiltonians are quadratic in creation and annihilation operators, one can use their matrix representation to find the optimal control sequences.

As a simple example, we discuss how to prepare the ground state of a hopping Hamiltonian on three orbitals,

$$\mathcal{H}_{J_X} = \frac{1}{\sqrt{2}} \left( c_2^\dagger c_1 + c_3^\dagger c_2 + \text{h.c.} \right). \quad (\text{C1})$$

Besides  $\mathcal{H}_{J_X}$ , we also need  $\mathcal{H}_{J_Z}$  in our control set,

$$\mathcal{H}_{J_Z} = c_1^\dagger c_1 - c_3^\dagger c_3, \quad (\text{C2})$$

whose ground states are easy to prepare. Using the normal ordered form in Eq. (A3), we have the matrix representations for  $\mathcal{H}_{J_X}$  and  $\mathcal{H}_{J_Z}$ ,

$$J_X = \frac{1}{\sqrt{2}} \begin{pmatrix} 0 & 1 & 0 \\ 1 & 0 & 1 \\ 0 & 1 & 0 \end{pmatrix}, \quad J_Z = \begin{pmatrix} 1 & 0 & 0 \\ 0 & 0 & 0 \\ 0 & 0 & -1 \end{pmatrix}, \quad (\text{C3})$$

which are the same as the corresponding spin-1 angular momentum operators. Using two rotations along the  $X$ -

axis and the  $Z$ -axis, we have

$$J_X = e^{-i\pi J_Z/2} e^{-i\pi J_X/2} J_Z e^{i\pi J_X/2} e^{i\pi J_Z/2}. \quad (\text{C4})$$

Using the isomorphism (A6), one can prepare eigenstates of the hopping Hamiltonian  $\mathcal{H}_{J_X}$  by applying  $\mathcal{U}$  to the corresponding eigenstates of  $\mathcal{H}_{J_Z}$ , where

$$\mathcal{U} = \exp(-i\pi \mathcal{H}_{J_Z}/2) \exp(-i\pi \mathcal{H}_{J_X}/2). \quad (\text{C5})$$

Since  $J_Z$  is diagonal, the eigenstates of  $\mathcal{H}_{J_Z}$  are easy-to-prepare Slater determinants in the computational basis (3).

As a second example, we discuss the permutation of orbitals,

$$\begin{pmatrix} 1 & 2 & 3 \\ 3 & 2 & 1 \end{pmatrix}, \quad (\text{C6})$$

which requires three FSWAP gates on neighboring qubits in the JWT. We show how it can be achieved with a single multi-qubit gate using Hamiltonian evolution by  $\mathcal{H}_{J_X}$ . The matrix powers of  $J_X$  are

$$J_X^2 = \frac{1}{2} \begin{pmatrix} 1 & 0 & 1 \\ 0 & 2 & 0 \\ 1 & 0 & 1 \end{pmatrix}, \quad J_X^3 = J_X. \quad (\text{C7})$$

From Eq. (C7), we can derive the exponential of  $J_X$ ,

$$e^{-i\tau J_X} = 1 - i \sin \tau J_X + (\cos \tau - 1) J_X^2. \quad (\text{C8})$$

For  $\tau = \pi$ , we have

$$e^{-i\pi J_X} = 1 - 2J_X^2 = - \begin{pmatrix} 0 & 0 & 1 \\ 0 & 1 & 0 \\ 1 & 0 & 0 \end{pmatrix}. \quad (\text{C9})$$

Therefore, the unitary that swaps the first orbital with the third orbital equals to

$$\mathcal{F}_{\text{swap}}^{1,3} = \exp \left( -i\pi \sum_{j=1}^3 c_j^\dagger c_j \right) \exp(-i\pi \mathcal{H}_{J_X}), \quad (\text{C10})$$

where the first term on the right-hand side fixes the extra minus sign in Eq. (C9). The two constituent parts in Eq. (C10) commute to each other, and the first part can be implemented with only single-qubit gates with the JWT.

### Appendix D: Fermionic SWAP gate

The fermionic swap (FSWAP) gate on two neighboring qubits takes the form [36],

$$F_{\text{swap}}^{q,q+1} = \begin{pmatrix} 1 & 0 & 0 & 0 \\ 0 & 0 & 1 & 0 \\ 0 & 1 & 0 & 0 \\ 0 & 0 & 0 & -1 \end{pmatrix}, \quad (\text{D1})$$

where we use the standard order of basis states  $|00\rangle, |01\rangle, |10\rangle, |11\rangle$ . One way to implement the fermionic SWAP gate is to use the ISWAP gate

$$\text{ISWAP} = \begin{pmatrix} 1 & 0 & 0 & 0 \\ 0 & 0 & i & 0 \\ 0 & i & 0 & 0 \\ 0 & 0 & 0 & 1 \end{pmatrix} = e^{\frac{i\pi}{2} H_{\text{iswap}}^{q,q+1}}, \quad (\text{D2})$$

$$H_{\text{iswap}}^{q,q+1} = \frac{1}{2} (X_q X_{q+1} + Y_q Y_{q+1}). \quad (\text{D3})$$

To fix the phases in ISWAP, we introduce

$$e^{\frac{i\pi}{4}(Z_q + Z_{q+1})} = \begin{pmatrix} i & 0 & 0 & 0 \\ 0 & 1 & 0 & 0 \\ 0 & 0 & 1 & 0 \\ 0 & 0 & 0 & -i \end{pmatrix}, \quad (\text{D4})$$

which commutes with the ISWAP gate. The fermionic SWAP gate then takes the form

$$F_{\text{swap}}^{q,q+1} = -i e^{\frac{i\pi}{4}(Z_q + Z_{q+1})} e^{\frac{i\pi}{2} H_{\text{iswap}}^{q,q+1}}. \quad (\text{D5})$$

### Appendix E: Simulating the 2D Hubbard model with a qubit ladder

Experimentally, it is often easier to build qubits on a ladder (two coupled chains) than on a 2D lattice. The two spin chains in a ladder can be used to map fermionic modes with two different spin states; see Fig 18. Because there are no hopping terms between the two spin states in the Hubbard model, the quantum state can be mapped using two independent JWTs on the two spin chains. One only needs to implement hopping terms within the chains and interaction terms between corresponding qubits in the two chains. In Ref. [62], the authors discussed physical implementations of analog quantum simulators of the 1D Hubbard model on a qubit ladder. Here, we discuss digital quantum simulation of the 2D Hubbard model using the same architecture. The challenge is to implement both the horizontal and vertical hopping terms with only local qubit operations. We solve this problem by reordering the spin orbitals encoded in the JWT using the fermionic SWAP gate (see Appendix D). Similar ideas have been proposed independently by Kivlichan *et al.* [42].

We will demonstrate our approach using an example, where the Fermi-Hubbard model on a  $3 \times 3$  lattice is mapped to a qubit ladder of size  $2 \times 9$ , see Fig. 18. The spin-up (down) orbitals are mapped to the upper (lower) chain in the ladder using the JWT. To implement both the horizontal and vertical hopping terms, one can switch between row-major and column-major orders,

$$\begin{pmatrix} 1 & 2 & 3 \\ 4 & 5 & 6 \\ 7 & 8 & 9 \end{pmatrix} \xrightarrow{\text{transposition}} \begin{pmatrix} 1 & 4 & 7 \\ 2 & 5 & 8 \\ 3 & 6 & 9 \end{pmatrix}, \quad (\text{E1})$$

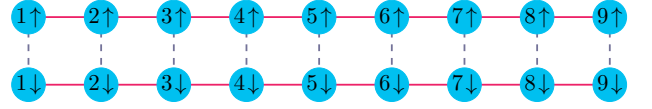


FIG. 18. A  $2 \times 9$  qubit ladder (two chains) is used to simulate the 2D Hubbard model on a  $3 \times 3$  lattice. The spin-up and -down orbitals are mapped to the upper and lower qubit chains, respectively, using two independent JWTs. The solid red lines represent nearest-neighbor interactions between qubits in the same JWT, and a dashed blue line represents  $ZZ$  interactions between qubits representing different spin states.

which corresponds to the following in-situ transposition of the fermionic orbitals in the JWT:

$$\begin{pmatrix} 1 & 2 & 3 & 4 & 5 & 6 & 7 & 8 & 9 \\ 1 & 4 & 7 & 2 & 5 & 8 & 3 & 6 & 9 \end{pmatrix}. \quad (\text{E2})$$

This permutation can be decomposed into elementary permutations involving only neighboring qubits; see Fig. 19. The pink-colored permutation in Fig. 19 can be

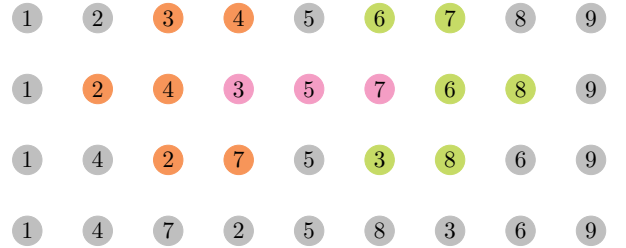


FIG. 19. The in-situ matrix transposition (E2) can be decomposed into elementary fermionic permutations involving only neighboring qubits (time goes from top to bottom). The first line is the initial ordering and the last line is the target ordering. In each line, the qubits plotted with the same bright color are involved in one elementary permutation, and their positions are updated in the next line. The gray qubits remain in the same place. The pink-colored permutation can be implemented with three FSWAP gates involving only neighboring qubits, or by Hamiltonian evolution as described in Appendix C. The rest of the permutations require a single FSWAP gate.

implemented using three FSWAP gates involving only neighboring qubits; in Appendix C, we discuss an alternative approach to implement this permutation using Hamiltonian evolution. The number of two-qubit gates required to implement the in-situ transposition for the two chains is  $N_{\text{trans}} = 2 \times 9 = 18$ . The numbers of two-qubit gates needed for the on-site interaction terms and the hopping terms are  $N_{\text{int}} = 9$  and  $N_{\text{hop}} = 2 \times 2 \times 6 = 24$ , respectively. The total number of two-qubit gates needed to simulate a single Trotter step is  $N_{\text{trott}} = N_{\text{trans}} + N_{\text{int}} + N_{\text{hop}} = 51$ .

To end this Appendix, we consider simulating the 2D Fermi-Hubbard model on a lattice of dimension  $n_x \times n_y$  using a qubit ladder of length  $n_x n_y$ . Without loss of

generality, we assume that  $n_y \geq n_x$ . The fermionic orbitals are mapped to qubits in row-major order using the JWT. Implementing the in-situ matrix transposition on the entire chain requires  $O(N^2)$  two-qubit gates and is inefficient. Instead, we can implement the in-situ matrix transposition on orbitals in neighboring rows. This modification allows one to implement all the hopping terms on a lattice with only  $O(N^{1.5})$  two-qubit gates. For example, a single Trotter step can be implemented with 7 constituent operations:

1. Implement the horizontal hopping terms and the on-site interaction terms,
2. Implement in-situ transpositions on spin orbitals in the 1st and 2nd rows, 3rd and 4th rows, and so on,
3. Apply vertical hopping terms between these pairs of rows,
4. Undo the in-situ transposition,
5. Implement in-situ transposition on spin orbitals in the 2nd and 3rd rows, 4th and 5th rows, and so on,
6. Apply vertical hopping terms between these pairs of rows,
7. Undo the in-situ transposition.

A single in-situ transposition involving two rows requires  $(n_x - 1)n_x/2$  FSWAP gates on neighboring qubits to implement. Because there are  $4(n_y - 1)$  in-situ transposition in one Trotter step, the total number of two-qubit gates required for that is  $N_{\text{trans}} = 2(n_y - 1)(n_x - 1)n_x = Nn_x - N - 2n_x^2 + 2n_x$ , where  $N = 2n_y n_x$  is the total number of spin orbitals. The numbers of two-qubit gates needed for the on-site interaction terms and the hopping terms are  $N_{\text{inter}} = N/2$  and  $N_{\text{hop}} = 2(n_y - 1)n_x + 2(n_x - 1)n_y = 2N - 2(n_y + n_x)$ , respectively. For square lattices, the total number of two-qubit gates needed for a single Trotter step is  $N_{\text{trott}} = N_{\text{trans}} + N_{\text{inter}} + N_{\text{hop}} \simeq N^{3/2}/\sqrt{2} + N/2$ . For example, the total number of two-qubit gates is 275 for 50 spin orbitals on a square lattice of size  $5 \times 5$ .

## Appendix F: Numerical study of the Trotter error

One way to prepare strongly correlated quantum states is by adiabatic evolution. On a digital quantum computer, we can simulate the evolution by dividing it into discrete time steps and approximating the Hamiltonian within each time step. Here, we numerically study the errors that arise from using a second-order Trotter formula

to simulate adiabatic state preparation for the ground states of the Fermi-Hubbard model.

For simplicity, we only consider the hopping and interaction terms:

$$\mathcal{H}_{\text{hop}} = - \sum_{\langle j,k \rangle, \sigma} t_{jk} (c_{j,\sigma}^\dagger c_{k,\sigma} + \text{h.c.}), \quad (\text{F1})$$

$$\mathcal{H}_{\text{int}} = U \sum_j n_{j,\uparrow} n_{j,\downarrow} - \mu \sum_{j,\sigma} n_{j,\sigma}. \quad (\text{F2})$$

We have introduced a chemical potential term in  $\mathcal{H}_{\text{int}}$  to fix the particle number of the ground state so that it occurs at half filling. Since the ground state of  $\mathcal{H}_{\text{hop}}$  is also half-filled and both  $\mathcal{H}_{\text{hop}}$  and  $\mathcal{H}_{\text{int}}$  conserve particle number, the particle number stays constant throughout the evolution. To prepare a ground state of  $\mathcal{H}_{\text{int}}$  starting from a ground state of  $\mathcal{H}_{\text{hop}}$ , we would apply the time-dependent Hamiltonian

$$\mathcal{H}(s) = (1 - s)\mathcal{H}_{\text{hop}} + s \cdot \mathcal{H}_{\text{int}}, \quad (\text{F3})$$

where  $s = t/T \in [0, 1]$  with  $T$  the total evolution time. If we split the total evolution time into  $n$  steps, then a single Trotter step takes the form

$$e^{-i(1-s)\Delta t \mathcal{H}_{\text{hop}}} e^{-is\Delta t \mathcal{H}_{\text{int}}}, \quad (\text{F4})$$

where  $\Delta t = T/n$ .

For the purposes of this study, we ignored the issue of approximating the two time-evolution operators in Eq. (F4). We used the parameter settings

$$\begin{aligned} t_{jk} &= 1 \text{ for all } j, k, \\ U &= 4, \text{ and} \\ \mu &= 1, \end{aligned}$$

on 2-dimensional grids of various sizes. We used the open-source package OpenFermion [37] to initialize the Hamiltonians (F2) and compute their ground states. Then, we used the open-source package QuTiP [63] to compute the exact evolution by the time-dependent Hamiltonian (F3), starting with the ground state of  $\mathcal{H}_{\text{hop}}$ . We adjusted the total evolution time  $T$  until the final state was within the ground space of  $\mathcal{H}_{\text{int}}$ , indicating that the evolution was adiabatic. For all the grid sizes we studied,  $T = 100$  was sufficient. Finally, we approximated the evolution using the second-order Trotter formula with various values of  $n$ , the number of steps. Higher values of  $n$  give a better approximation. For each step size, we recorded the quantum state 20 times throughout the evolution and computed the fidelity of these states with the states from the true adiabatic evolution. The numerical results are shown in Fig. 20.

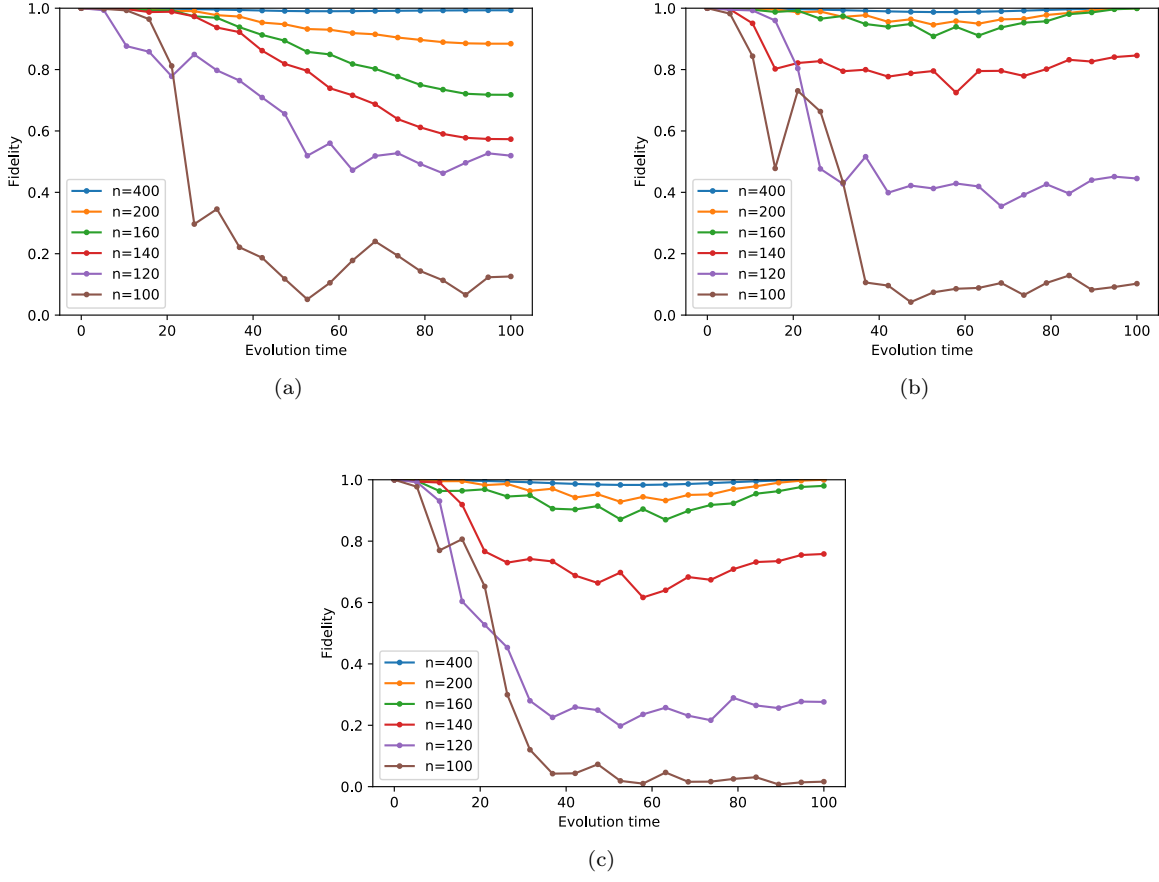


FIG. 20. Fidelity with states from adiabatic evolution for various Trotter step numbers. (a): 2-by-2 grid. (b): 3-by-2 grid. (c): 4-by-2 grid.